Continental weathering in the Early Triassic in Himalayan Tethys, central Nepal: Implications for abrupt environmental change on the northern margin of Gondwanaland

Kohki Yoshida[1], Toshio Kawamura[2], Shigeyuki Suzuki[3], Amar Deep Regmi[4], Babu Ram Gyawali [5], Yuka Shiga[1], Yoshiko Adachi [7] and Raj Megh Dhital [4]

[1]Department of Geology, Faculty of Science, Shinshu University, Matsumoto 390-8621, Japan, kxyoshid@shinshu-u.ac.jp

[2] Department of Earth Science, Miyagi University of Education, 980-0845, Japan

[3] Department of Earth Science, Okayama University, Okayama 700-8530, Japan

[4] Central department of Geology, Tribhuvan University, Kritipur, Kathmandu, Nepal

[5] Department of Earth Science, Tohoku University, Sendai, 980-8578, Japan

[6] Chiyoda Corporation, Yokohama, 220-8765, Japan

[7] Department of Geology, Faculty of Science, Niigata University, Nigata 950-2181, Japan

ABSTRACT

The geochemistry of Triassic mudstones in the Himalayan Tethys sequence, central Nepal, was studied with respect to changes in sedimentary facies, grain size, and source rocks. The Triassic sedimentary facies of mudstone and carbonates show deposition in offshore to hemiplegic environments. The rare earth element (REE) pattern of the Permian and Triassic mudstones suggests uniformity correlatable to average shale. The major element geochemistry of the Early Triassic Griesbachian–early Smithian mudstones indicates a sediment supply from strongly weathered sources with the chemical index of alteration (CIA) values of 76–81. However, the mudstones in the late Smithian show weakly weathered sources with CIA values of 68–74. The lower part of the Middle Triassic Anisian mudstones return to Early Triassic paleoweathering levels. There are no significant relationships among lithofacies, the grain size of the sediments, and CIA values. Thus, the abrupt change of the degree of paleoweathering in the Early Triassic, late Smithian time, suggests a dramatic decrease in continental weathering, which is related to a predominantly arid climate in the northern marginal area of Gondwana.

INTRODUCTION

The end-Permian mass extinction in the late Paleozoic era, approximately 250 million years ago, marked the disappearance of the typical end-Paleozoic faunas, which dramatically affected the evolution of life (Erwin, 1993; Raup and Sepkoski, 1982; Hallam, 1991). A significantly delayed recovery of marine and terrestrial biota is considered to have continued into the initial part of the Middle Triassic (Anisian period) (Erwin, 1993; Hallam, 1991). The failure of most communities to flourish during the Early Triassic indicates the persistence of harsh conditions (Hallam, 1991; Dickins, 1993). For example, metazoan reef systems (Senowbari-

Daryan et al., 1993), forest ecosystems (Looy et al., 1999), and seafloor communities (Hallam and Wignall, 1997) showed recovery difficulties in the Early Triassic. Most studies investigating this period suggest that the delay in recovery may be attributed to the persistence of unfavorable climatic and/or oceanographic conditions such as an intense hothouse climate, acidification of the ocean, or ocean anoxia (Erwin, 1993; Hallam and Wignall, 1997; Wignall and Twitchewtt, 2002). However, several marine faunas including conodonts and ammonoids diversified explosively in the initial part of the Early Triassic (Brayard et al., 2006, 2009; Orchard, 2007).

In the last decade, the focus of research has expanded from the extinction event at the Permian–Triassic (P/T) boundary to the mode and environmental conditions during ecosystem recovery in marine and terrestrial environments. The timing and key factors contributing to this recovery have been broadly studied (e.g., Knoll et al., 2007; Payne et al., 2010). Recently, Hermann et al. (2011, 2012) reported palynological and particulate organic matter data from the Early Triassic in Pakistan and South Tibet. However, few studies have discussed the environmental changes, including weathering in terrestrial environments at mid-latitudes in the Early Triassic, except for those at the P/T boundary, although definitive evidence regarding reconstruction of paleosols and faunal provinces is reported (e.g., Bourquin et al., 2011).

The aim of the present study is to provide constraints on environmental changes on the basis of the geochemical composition of mudstones during the Early Triassic in a well-dated succession. For this purpose, sedimentary sequences were selected from the Manang area of the Tethyan Himalayas, central Nepal (Figs. 1-A and B), which was located in the mid-paleolatitudes and faced the Neo–Tethys Ocean in the southern hemisphere (Golonka and Ford, 2000). In addition, the elemental ratio of terrigenous material is very important in estimating weathering conditions in the hinterlands. Because CaO, which is a primal component of carbonates, disturbs the elemental ratio of soluble–insoluble elements in terrigenous materials, mudstone geochemistry is utilized in this study.

REGIONAL GEOLOGY

The stratigraphy and structure of the selected sections of the Permian and Triassic sequences in the Manang area, Tethyan Himalaya, central Nepal have been studied previously (Bordet et al., 1975; Bassoullet and Colchen, 1977; Fuchs, 1977; Fuchs et al., 1988; Garzanti et al., 1994a; von Rad et al., 1994; Baud et al., 1996). The geology has been classified into the following four geological units: Permian Puchenpra Formation, “topmost biocalcarenites,” Lower Triassic Tamba Kurkur Formation, and Middle–Upper Triassic Mukut Formation.

These sequences are stratigraphically constrained in this area by conodont and ammonoid fossils (Bordet et al., 1975; Bassoullet and Colchen, 1977; Fuchs et al., 1988; Garzanti et al., 1994a, b; Waterhouse, 2010). The Lower Triassic Tamba Kurkur Formation in the Manang area is stratigraphically well constrained by index fossils such as conodonts (Garzanti et al., 1994a, b) and consists of the following stages (Fig. 1-C): Griesbachian, which includes the topmost biocalcarenites and first carbonate band; Dienerian, which primarily represents the first mudstone interval; Smithian, which primarily includes the second carbonate band; and Spathian, which represents the second mudstone interval and third carbonate band. Major facies and ages are described in the following paragraph.

Puchenpra Formation

This formation, which was separated from the Thini Chu Group by Garzanti (1999), consists of quartz sandstone and mudstone with limestone–marl intercalations. The Kuling

Group of the Spiti–Zanskar area is equivalent to this formation (Garzanti et al., 1996b; Baud et al., 1996). The original definition of the Thini Chu Formation by Bodenhausen et al. (1964) included dark mudstones and white sandstones intercalated with richly bioclastic intervals of the Carboniferous age and “exceptionally ill-sorted sandstones.” Garzanti (1999) divided this formation into the Thini Chu Group of Carboniferous–lowermost Permian age and the Puchenpra Formation, which unconformably overlies the Thini Chu Group. The age of the Puchenpra Formation is considered to be from the Sakmarian/Artinskian to Wuchiapingian on the basis of calcareous benthic foraminifera (Colchen and Vachard, 1975), brachiopods, bivalves, and conodonts (Garzanti et al., 1994b). In the sample section, a 50-m-thick section below the top is cropped out.

Topmost biocalcarenites

A thin, distinct unit consisting of orange-bedded biocalcarenite with dolomitized micritic groundmass appears on the Puchenpra Formation (Bassoullet and Colchen, 1977). This unit is called the “Pangjang Formation” to ascribe to the basal Triassic (Waterhouse, 1977; 1994; Hatleberg and Clark, 1984; Baud et al., 1996) or the topmost biocalcarenites as a topmost part of the Puchenpura Formation (Garzanti et al., 1994a, b). Although the age range is Kubergandian–Murgabian, as indicated by brachiopods and conodonts at the base, the mixing of macrofossils and conodonts of Permian and Triassic ages occurs at the top of this horizon (Nicora and Garzanti, 1997). Because uncertainly in age and sedimentological characters still remain, the latter informal name (Garzati et al., 1994a) is used in the present study.

This unit, which is 1.1–2.5 m in thickness, consists of orange-weathered reddish biocalcareites, including brachiopods, fenestellid bryozoans, corals, crinoids, and bivalves, along with quartz grains.

Tamba Kurkur Formation

The age of the Tamba Kurkur Formation ranges from Griesbachian to upper Spathian or Anisian, according to the biostratigraphy of ammonoids and conodonts (von Rad et al., 1994; Garzanti et al., 1994a), and conformably overlies the topmost biocalcarenites. Its thickness is 60 m and is composed of marly limestone and mudstone.

Detailed stratigraphy has been established on the basis of conodonts, brachiopods, and ammonoids in the Manang area (Nicora et al., 1992; Garzanti et al., 1994a). The major index fossils (Garzanti et al., 1994a) and lithofacies are shown in Fig. 1-C. The lithological characteristics in the study area suggest that this Lower Triassic system can be classified into six lithological units composed of three carbonate bands (first, second, and third carbonate bands) and two mudstone intervals (first and second mudstone intervals).

Mukut Formation

The Mukut Formation in the Manang area consists of a 200-m-thick sequence of limestone and shale from Anisian to late Carnian in age (Garzanti et al., 1994a). In the sample section, a 40-m interval in the lower part of the Mukut Formation is observed. The limestone consists of bioclastic wackestones and marlstones and includes foraminifera, ostracods, echinoderms, ammonites, and brachiopods.

Biostratigraphy

Several important fossils have been reported (Garzanti et al., 1994a; Waterhouse, 2010) in the Lower Triassic strata near the Manang area. Waterhouse (2010) reported basal Triassic, Griesbachian ammonoids *Otoceras woodwardi* and *Ophiceras tibeticum* from the topmost biocalcarenites. The first carbonate band of the Tamba Kurkur Formation (Fig. 1-C-1) yielded Griesbachian conodonts, including *Hindeodus* cf. *typicalis* Sweet, 1970, and *Gondolella carinata* Clark, 1959. In the first mudstone interval (Fig. 1-C-2), early Dienerian conodonts, *Gondolella nepalensis* Kozur & Mostler, 1976, were recovered from the lower part and Late Dienerian–early Smithian *Nepspathodus pakistanensis* Sweet, 1970 were found in the upper part in the Manang area. The second carbonate band (Fig. 1-C-3 and 4) yielded *N. pakistanensis*, *N. waageni* Sweet, 1970, and *Gondolella sweeti* Bender, 1970, suggesting a Smithian age. The thin mudstone interval (Fig. 1-C-5) between the second and third carbonate bands yielded *Gondolella*. aff. *Jubata*, Bender, 1970, suggesting a late Smithian age. From the third carbonate band (Fig. 1-C-6), late Smithian–late Spathian conodonts, *G*. aff. *Jubata*, *Neospathodus homeri* Bender, 1970, *Gladigondolella carinata* Bender, 1970, and *Neospathodus spathi* Bender, 1970, have been observed. *Gondolella timorensis* Bender, 1970, which was found at the top of the third carbonate band (Fig. 1-C-7) by Garzanti et al. (1994a), indicates the late Spathian (Goudemand et al., 2012). The lower part of the Mukut Formation in the Manang area yielded Early Anisian fossils (Garzanti et al., 1994a) such as conodonts: *Gondolella regalis* (Mosher, 1970); brachiopods: *Punctospirella stracheyi* and "*Dielasma*" *himalayanum*; and ammonoids: *Hoolandites* sp.

Recently, the Tulong Formation in South Tibet, which has very similar lithology as the Tamba Kurkur Formation in the Manang area, was revised by Brühwiler et al. (2009) using ammonoids and conodonts. The stratigraphy of the Tulong Formation suggests that the first carbonate ranges from middle to late Smithian and the second mudstone interval is Spathian (Brühwiler et al., 2009). Thus, the chronological framework of the Tamba Kurkur Formation in the Manang area proposed by Garzanti et al. (1994a) has been changed to include the above recent revision of the Triassic biostratigraphy.

FACIES DESCRIPTION IN THE SAMPLE SECTION

On the northern cliff of Manang village, the Lower Triassic deposits are well exposed and are easily accessible. The continuous sequence from the Permian Puchenpra Formation to Upper Triassic Mukut Formation was reported by Garzanti *et al*. (1994a), although the Mukut Formation, which is distributed over an altitude of 4500 m on the cliff, is not accessible. The abovementioned strata have an east–west trending strike and are nearly horizontal or gently dipping to the north–northwest (Fig. 2-A).

Permian Unit

Puchenpra Formation

The Puchenpra Formation in this section consists of approximately 50 m of alternating beds of sandstone and mudstone. The sandstone bed shows troughs and hummocky cross-stratification (HCS) (Fig. 2-B). The mudstone is intensely bioturbated and includes large U- and I-shaped burrows.

Triassic Unit

The Triassic unit consists of topmost biocalcarenites and the Tamba Kurkur and Mukut Formations. The Triassic Tamba Kurkur Formation is divided into five subunits (Fig. 1-C). The lower two units are mostly similar to that reported by von Rad et al. (1994) and Baud et al. (1996) for the Jomsom area, although the upper three units differ with respect to thickness and lithofacies.

Topmost biocalcarenites

Orange dolomitic sandy limestone, which is 1.1 m in thickness, lies above the uppermost part of the Puchenpra Formation (TB in Figs. 2-A and C). This dolomitic sandy limestone consists of stratified bioclastic wackestones and includes fine sand-sized quartz grains and calcareous bioclasts such as brachiopods, bryozoans, ostracods, small foraminiferans, and crinoids (Fig. 2-D). Individual beds show massive structures, including oversize clasts of bryozoans and brachiopods. The contact between the base of this unit and the mudstone of the uppermost part of the Puchenpra Formation shows a slightly deformed undulating plane, probably suggesting loading or erosional structures (Fig. 2-C).

Tamba Kurkur Formation

First carbonate band

The first carbonate band, which is located at the base of the Tamba Kurkur Formation, consists of orange- and gray-colored dolomitic limestone 3 m in thickness. At the base of this interval, several layers of 30–50-cm-thick orange dolomitic limestone rest on the orange dolomitic sandy limestone of the topmost biocalcarenites (TB in Fig. 2-C). Although the boundary between the topmost biocalcarenites and Tamba Kurkur Formation is a planar contact, there is no clear evidence of erosion. The limestone of the Tamba Kurkur Formation consists of fine bioclastic wackestone and mudstone, including thin-shelled bivalves and small ammonites without quartz grains. Although the gray wackestone that rests on the abovementioned bioclastic wackestone and mudstone is recrystallized and dolomitized, it still includes thin-shelled bivalves, small ammonoids, and radiolarians (Fig. 2-H). These limestone layers, along with the uppermost Permian (Tc1 + TB in Fig. 2-A), show distinctive marker horizons, which make them easily recognizable in the outcrop.

First mudstone interval

The first mudstone interval consists of 30-m-thick dark red–black mudstones. These mudstones contain thinly bedded, alternating layers of 1–10-mm-thick red–purple mudstone and black mudstone (Fig. 2-E). Small burrows approximately 5 mm in diameter are rarely observed (Fig. 2-F). The mudstone layer shows grading (Fig. 2-G). In the lower part of this mudstone interval, several thin-bedded orange dolomitic limestone layers are intercalated.

Second carbonate band

An 8–10 m thick, second carbonate band consists of gray–yellow nodular limestone with intercalated thin gray mudstone layers. In the lower part of this carbonate band, the yellow limestone is composed of wackestone–packstone containing numerous fragments of thin-shelled bivalves. In the upper part, the gray–yellow nodular limestone consists of wackestone–packstone with numerous ammonoids and thin-shelled bivalves (Fig. 2-I). The uppermost horizon of this unit consists of a peculiar packstone–grainstone containing large numbers of ostracods with ammonoids, gastropods, sponge spicules, and crinoids.

Second mudstone interval

The mudstone temporally intercalated between the second and third carbonate bands has no characteristic sedimentary structures such as wave ripple or HCS. This interval is a 20–30-cm-thick dark gray mudstone between the second and third carbonate bands. The thin beds of calcareous mudstone or muddy limestone are rarely intercalated. This mudstone consists of dark gray shales with weak bioturbation. Examination under a microscope reveals that the original thin lamination is preserved; however, such lamination is frequently disturbed by small burrows.

Third carbonate band

The third carbonate band consists of a 12-m-thick gray nodular limestone that includes ammonite-bearing gray nodular limestone and alternating beds of gray limestone and mudstone in the lower part. The gray limestone in the lower part is a wackestone containing ostracods and thin-shelled bivalves with some ammonoids (Fig. 2-J). The upper part consists of nodular gray limestone and reddish gray nodular limestone intercalated with thin gray and red calcareous mudstone. In this part, the limestone clearly includes small ammonites, ostracods, radiolarians, and thin-shelled bivalves along with fine sand-sized quartz grains. However, as previously mentioned, this horizon is intensely deformed and recrystallized (Fig. 2-K).

In the uppermost part of this unit, stratified limestone with a few mudstone intercalations gradually grade into thin-bedded alternating layers of limestone and mudstone in the lower part of the Mukut Formation (Fig. 2-L).

Interpretation of sedimentary environments

A total of five units reflect the main depositional environments through sedimentary structure, grain size, and bioturbation amount.

Puchenpra Formation

The sedimentary facies of the Puchenpra Formation indicate offshore environments located between storm and fair-weather wave bases. A large amount of bioturbation is appropriate for this environment.

Topmost biocalcarenites

In this unit, the lack of sedimentary structures that present in the shallow marine environment suggests deposition below storm wave base. Because this unit consists of an ill-sorted mixture of quartz grains and small and large fragments of bioclasts, they may be lag deposits with rapid transgression.

First carbonate band

This unit consists of massive wackestone and lime–mudstone with an absence of shallow marine sedimentary structures. This facies indicates a lower-energy environment offshore or deposition below the storm wave base.

First mudstone interval

Bioturbation is rare and small-scale laminations have been completely preserved in this unit. Grading and absence of shallow marine sedimentary structures indicate deposition in an offshore environment or that below the storm wave base.

Second carbonate band

The lithofacies of this unit is characterized by fossiliferous wackestone. In the lower part, a concentration of thin-shelled bivalve clasts reflects an episode of gregarious deposition at the sea bottom. In the upper part, nektonic and benthic fossils such as ammonoids and bivalves are prevalent as constituents of the limestone, indicating deposition in hemiplegic environments.

Second mudstone interval

Minor carbonate intercalations suggest a temporary decrease in carbonate productivity or of the input of prevailing terrigenous material. The absence of shallow marine sedimentary structures suggests deposition below the storm wave base or within a very short time interval.

Third carbonate band

The prevailing wackestone with benthic fossils and a lack of typical shallow marine sedimentary structures implies deposition in low-energy hydraulic bottom environment. The remaining structure of bivalve concentration suggests deposition in a pelagic environment. The intercalated red calcareous mudstone in the upper part may be correlated to the Ammonitico Rosso facies observed in the Jomsom area, central Nepal (von Rad *et al*., 1994) and Tulong area, South Tibet (Brühwiler et al., 2009). The sandy wackestone containing quartz grains may be indicative of temporal change of transporting patterns of sediments and rapid predominance of terrigenous material.

DESCRIPTION OF MUDSTONES IN THE SAMPLE SECTION

The mudstones of the Tamba Kurkur Formation can be described as weakly metamorphosed gray–black mudstones with lithologies ranging from claystone to coarse siltstone. Small-sized burrows ranging from 2–5 mm in diameter are occasionally included.

The quartzose and feldspathic grains in the mudstones are predominantly angular to subangular. Graded bedding is mostly obscured due to recrystallization and weak deformation. Deformation by compaction is observed, as evidenced by commonly deformed calcareous biogenic spherical grains.

The characteristics of these mudstones, in conjunction with petrographic observations revealed under a microscope, indicate the following characteristics:

1. The mudstones in the Puchenpra Formation are matrix-supported siltstones with very fine quartz grains. Quartz grains are angular–subangular. In addition, biotite, white mica, and tourmaline grains are included. Calcareous grains originating from the fragments of calcareous organisms are frequently included. Authigenic rhombohedral dolomite grains are commonly observed.

2. The mudstone in the first mudstone interval of the Tamba Kurkur Formation is fine siltstone to claystone with quartz grains 0.005–0.35 mm in diameter, with an average grain size

of 0.017–0.029 mm (Fig. 3-a and b). Although slaty cleavage is present, the sample contains detrital muscovite flakes that are locally oblique to the cleavage of the metamorphic mica minerals. Occasionally, detrital calcite or biogenic calcite grains are included. Authigenic dolomite and pyrite grains can be observed. Several mudstones, which consist of coarse-grained minerals of metamorphic chlorite and mica, are intercalated in the first mudstone interval.

3. The mudstones in the second carbonate band are composed of thin layers intercalated with limestone. These mudstones are fine siltstones to claystones containing fine quartz and feldspar grains of 0.005–0.04 mm in diameter, with an average grain size of 0.014–0.021 mm (Fig. 3-c and d). Detrital muscovite is rare but present. The abundance of authigenic dolomite grains increases.

4. The mudstones derived from the third carbonate band are fine siltstones to claystones with quartz grains of 0.005–0.03 mm in diameter. Detrital muscovite is rare. Authigenic dolomite grains are included, along with metamorphic chlorite and mica minerals.

RESULTS OF GEOCHEMISTRY

Carbon isotope record in the Lower-Middle Triassic carbonate in Manang area

In this study, Early Triassic $\delta^{13}C_{carb}$ data from the Manang area, which is constrained by conodont stratigraphy (Garzanti *et al*., 1994a), are presented. Because samples of the Lower Triassic Tamba Kurkur Formation display very low $\delta^{18}O_{carb}$ values, with an average value of −12‰, and unusually low $\delta^{13}C_{carb}$ values during the Griesbachian to late Smithian, with an average value of −1.5‰ (Fig. 3), one may question whether the primary marine characteristics have been preserved or whether the measured isotope values represent diagenetic effects. Garzanti *et al*. (1994a, 1998) suggests that there may be some significant influence from diagenesis and metamorphism in the Permian/Triassic sections in South Tibet and the Manang area. In particular, significant metamorphic conditions are indicated by illite crystallinity, vitrinaite reflectance, and conodont color in the Manang area (Garzati *et al*., 1994a). A comparison between the $\delta^{13}C_{carb}$ and $\delta^{18}O_{carb}$ profiles show that $\delta^{18}O_{carb}$ varies with $\delta^{13}C_{carb}$ values in the second carbonate band, which suggests some influence of diagenesis on the isotope records. It is widely known that oxygen isotope values are more easily altered during diagenesis than carbon isotope values (Marshall, 1992). In the Tethyan Himalayas, very low $\delta^{18}O_{carb}$ values have been found and explained by thermal metamorphism of up to 300 °C (Baud *et al*., 1996; Atudorei and Baud, 1997). However, it is known that relative changes in the carbon isotope excursion are preserved in low-grade metamorphic conditions and that the signal can be correlated with other records for the same time span, as shown in other Himalayan sections (Baud *et al*., 1996; Atudorei and Baud, 1997; Brühwiler *et al*., 2009), although oxygen isotope values have been altered during diagenesis and metamorphism.

A bulk carbonate carbon isotope curve generated for the lower and upper parts of the Tamba Kurkur Formation shows a positive excursion. This correlation is discussed subsequently.

Inorganic geochemistry

The samples studied have been categorized into the following six groups: (1) mudstones intercalated in the Permian Puchenpra Formation, (2) mudstones in the topmost biocalcarenites, (3) the first mudstone interval, (4) mudstones intercalated in the second carbonate band, (5) mudstones in the third carbonate interval of the Tamba Kurkur Formation, and (6) mudstones in the lowermost horizon of the Mukut Formation.

In Fig. 5, Al_2O_3, Fe_2O_3*, MnO, and MgO concentrations generally show strong negative correlations with SiO_2. The wide compositional variety of the mudstones in the first mudstone interval tends to mask the characteristics of the mudstones in the other stratigraphic units. The mudstones in Permian and topmost biocalcarenites show lower concentrations of Al_2O_3, MgO, Fe_2O_3*, and P_2O_5 and higher concentrations of Na_2O and CaO, which are caused by its sandy nature with extended feldspar grains. The mudstones from the first mudstone interval appear to have a similar elemental composition to the third carbonate band and Mukut Formation. This interval also includes two samples that are characterized by high Fe_2O_3* and MnO concentrations and low SiO_2 and Na_2O concentrations. This is due to the high content of mica and Fe-oxide minerals. The mudstones in the second carbonate band show higher SiO_2, CaO, Na_2O, and P_2O_5 concentrations and lower concentrations of Al_2O_3, Fe_2O_3*, and MgO compared with other mudstones, which distinguishes their siliceous nature with lower alumina and iron contents.

Rare Earth Elements (REEs)

The average REE pattern shows that all six groups of sediments have similar chondrite-normalized REE patterns with overlapping abundances (Fig. 6). The concentrations show an increase in order of magnitude from Permian sediments and the second carbonate band to the first mudstone interval, the third carbonate band of the Triassic Tamba Kurkur Formation, and the Mukut Formation within a very narrow range. All groups of sediments show fractionated, parallel to subparallel REE patterns, with (La/Yb)N ratios ranging from 13.8 to 16.9 (Supplemental Table 1). Both LREE and HREE show variable fractionation with (La/Sm)N values ranging from 4.8 to 5.1. The (Gd/Yb)N value ranges from 1.6 to 1.9. This indicates that the REE content among various groups of mudstones varies within a narrow limit and that their fractionation is not large because the differences in both (La/Sm)N and (Gd/Yb)N ratios are of the same order of magnitude. All samples show consistently uniform negative Eu anomalies. The samples of the Tamba Kurkur and Mukut Formations do not show Ce anomalies, although Permian and topmost biocalcarenites samples show weakly positive Ce anomalies. Note that the REE patterns of the Triassic mudstones are similar to those of post-Archean Australian average shale (PAAS; Fig. 6), including the negative Eu anomalies. The patterns, which are comparable to PAAS, imply that the detrital material was derived from a common continental source.

Chemical weathering degree

It is widely accepted that marine mudstones preserve information about their sedimentary environments and hinterlands (Potter et al., 2005). In particular, information regarding terrestrial environments such as climatic conditions can be estimated by examining the paleoweathering of these rocks to determine the extent of chemical weathering. In general, warm and wet climates provide ample moisture for the hydrolysis of common elements such as Ca, Mg, Na, and K from surface rocks and soil minerals in the most weathered parts of the soil. On the contrary, arid and cool climates contain insufficient water for flushing cations from the soil into the groundwater. As a result, alkaline earth cations such as Ca and Mg remain within the soil as subsurface nodules (Retallack, 2005). Thus, several geochemical indices for estimating weathering effects, including CIA (Nesbitt and Young, 1982), have been used to derive transfer functions for paleoclimate estimation from sediments. In this study, CIA values along with Al_2O_3/Na_2O ratios are used to estimate degrees of weathering.

In the Manang area, which includes most of the Upper Permian to Lower Triassic sequence, the geochemical indices suggest significant vertical compositional variations (Fig. 7 and Supplemental Table 2). Most Lower Triassic sediments in the first mudstone interval of the Tamba Kurkur Formation show fairly constant CIA values and Al_2O_3/Na_2O ratios of 72–78 (average = 76.2, s.d. = 1.9) and 21–31 (average = 26.8, s.d. = 2.7), respectively. Four samples obtained from the upper part of the first mudstone interval and from the lower part of the second carbonate band show the CIA values of 67–69 (average = 68.1, s.d. = 1.3) and Al_2O_3/Na_2O ratios of 12–16 (average = 13.6, s.d. = 1.9; Fig. 7). From the third carbonate band of the Tamba Kurkur Formation to the Mukut Formation, the CIA values and Al_2O_3/Na_2O ratios were relatively higher, reaching 80 and 30, respectively. The index of compositional variability (ICV) values, which indicate the maturity of fine alumino–siliciclastic materials (Cox et al., 1995), were relatively constant with some minor fluctuations throughout the sample section, including exceptional two values in the lowest horizon of the section (<0.5) and in the first mudstone interval (>1.5).

Grain-size analysis

In the Tamba Kurkur Formation, the average grain size measured from mudstones ranged from 0.017 mm in the lower part of the first mudstone interval to 0.029 mm in the middle part of the same interval. However, a sample from the uppermost part of the Puchenpra Formation contained a coarser grain size of 0.043 mm. In contrast, samples from the upper part of the first mudstone interval and third carbonate band showed no significant differences in grain size.

DISCUSSION

Carbon isotope chemostratigraphy

The Triassic bulk carbon isotope data of the study area correlates to the Lower Triassic Tamba Kurkur Formation in the Tulong area, South Tibet (Brühwiler et al., 2009). These strata, which are distributed in the Tulong area, had been emended from the Tulong Formation by Garzanti *et al*. (1998). The lithostratigraphy of the Tamba Kurkur Formation in the Manang area is closely correlated to that of the Tulong area. The generated excursion of the Tamba Kurkur Formation in the Manang area shows considerable correlation with that in the Tulong area. On the basis of the correlation potential of the isotope curve between both areas, we differentiated four excursion types: prominent negative excursion (−5‰) around the P/T boundary, significant positive excursion (+3‰) at the Smithian–Spathian boundary (horizon A in Fig. 1-C), positive to negative excursion around the lower Spathian (horizon B in Fig. 1-C), and gentle positive excursion in the upper Spathian (horizon C in Fig. 1-C). Thus, combined correlations based on conodont presence and carbon isotope records in the Tulong area suggest that the approximate age of the horizon with low CIA values and Al_2O_3/Na_2O ratios is upper Smithian.

Record of sea level change

The sediments of the Lower Triassic show very thin thicknesses of approximately 50 m from Griesbachian to Spathian, representing a highly condensed sequence. The Lower Triassic sequence in the Tethys Himalayas is characterized by similar condensed sequence (von Rad et al., 1994; Baud et al., 1996; Galfetti et al., 2007a; Brühwiler et al., 2009). Although the thickness of stratigraphic succession always demands the consideration of tectonism and eustasy, the condensed sequence in a wide area of the Tethys Himalayas indicates that the sedimentation represents global sea level change that occurred during a transgressive stage. The cyclic sedimentation of carbonates and mudstone can be considered as a reflection of eustatic sea level changes in the sample section. The carbonate bands in the sample section could be correlated to the transgressive phase of the global cycle chart by Haq et al. (1988), Hardenbol et al. (1998), and Haq and Shutter (2008) (Fig. 1-C). The topmost biocalcarenites includes a large amount of bioclasts such as corals, bryozoans, and brachiopods with quartz grains, which is indicative of sediment reworking. Moreover, the transition from the Permian Puchenpura Formation to the topmost biocalcarenites is marked by a sharp erosional surface and a change of lithofacies from alternation of sandstone and mudstone to dolomitic orange sandy carbonate. Thus, the onset of the sedimentation of the Triassic system is interpreted to be related to starvation and subaqueous reworking of the sediments during early Griesbachian rapid transgression. The first carbonate band of the Tamba Kurkur Formation, directly overlying the topmost biocalcarenites, could be correlated to a highstand system tract in Griesbachian highstand. The first mudstone interval, which is rich in terrigenous material, likely suggests the lowstand systems tract in Dienerian and early Smithian because the input of terrigenous material was increased due to exposure of the shelf. The second and third carbonate bands could be correlatable to the late Smithian highstand and middle–late Spathian transgressive highstand system tracts, respectively. The second mudstone interval is likely correlative to the lowstand system tract with early Spathian regression.

Similar eustatic cycles are known from the Canadian Sverdrup Basin (Embry, 1997) and are recognized in many other sections such as the Western Tethys (Gianolla and Jacquin, 1998), Barents Sea (Gianolla and Jacquin, 1998; Skjold et al., 1998), and the Salt and Surghar Ranges (Hermann et al., 2011).

Provenance

Some elements, and particularly their ratios, are useful indicators of provenance because they are least affected by processes such as weathering, transport, and sorting. In particular, the common immobile elements such as REEs have been found to be useful (Taylor and McLennan, 1985). In addition, REEs are believed to preserve the composition of the source rock in which they are carried by the detrital component (Taylor and McLennan, 1985; Wronkiewicz and Condie, 1987). These elements indicate specific conditions in igneous petrogenesis. Hence, normalized REE patterns suggest low (La/Yb)N ratios and little or no Europium (Eu) anomalies in mafic rocks. In contrast, felsic rocks have higher (La/Yb)N ratios and significant Eu anomalies (Taylor and McLennan, 1985). The chondrite normalized REE patterns in all sediments in each unit of the sample section have been exactly fractionated and show significant Eu anomalies that suggest felsic source rock provenance.

The chondrite normalized REE patterns of the mudstones have been compared with those of PAAS. All patterns from the Triassic stratigraphic unit shown in this study are similar to that of the average shale. Moreover, these mudstones show enrichment of REE in comparison with PAAS. This feature implies that the REE patterns in each Triassic unit are neither affected by selective sorting in sedimentary process nor derived from different source rock types. Therefore, the enrichment requires a concentration of REE without significant changes in REE patterns. This process may be related to the elemental concentration due to chemical weathering, which leads to chemical leaching of soluble elements, leaving the insoluble elements in the hinterland. Cullers et al. (1987) indicated that the enrichment of REE in the clay fractions of stream sediments is relative to source rocks. They concluded that the REEs are released from primary minerals and taken up by the clay size fraction during chemical weathering of the source rock.

Paleoweathering record

The sediment chemistry indicates the results of the influence of transport processes, source rocks, and weathering (McLennan et al., 1983). The marine sediments reflect the characteristics of weathered source rocks and effects related to fluvial transportation and depositional environments. Thus, the compositions of initial detritus have been affected and modified by multiple factors such as climate, selective sorting in fluvial and marine processes, diagenesis, and metamorphism. Of these factors, the effects of diagenesis and metamorphism, which could not be completely excluded, are considered to be insignificant in this study because diagenetic and metamorphic alternations at specific horizons were not found in the sample section, which is indicated by the specific chemical composition and occurrence of authigenic mineral assemblages observed under a microscope. Although authigenic dolomite, metamorphic mica minerals, and iron minerals are observed in these rocks, biased bulk rock chemistry due to such specific mineral formation is not found.

The evolution of chemical weathering of sediments can reflect changes in the environment and may record the history of environmental changes in the depositional basin. It is widely accepted that weathering profiles have a significant effect on the geochemical compositions of siliciclastic sediments (Nesbitt and Young, 1982). Accordingly, the composition and subsequent CIA values of sediments can indicate the intensity of chemical weathering associated with climatic conditions (Nesbitt and Young, 1982; Fedo *et al*., 1997).

The uppermost horizon of the Permian strata of the Puchenpra Formation exhibited relatively variable CIA values of 67–73 and Al_2O_3/Na_2O ratios from 11 to 19. The topmost biocalcarenites represented CIA values of 69 and Al_2O_3/Na_2O ratios of approximately 16. However, most samples from the Tamba Kurkur Formation showed CIA values of 72–79, which are similar or slightly higher than those of PAAS and North American shale composite (NASC), i.e., 70–75 for average shales (Taylor and McLennan, 1985). These results suggest intense weathering conditions during the Griesbachian to Dienerian and early Smithian, even in the middle paleolatitudes, due to a hot–warm, humid climate, as indicated by previous paleontological and geochemical studies (Worsley et al., 1994; Kidder and Worsley, 2004). In contrast, the samples from the upper part of the first mudstone interval to second carbonate band (late Smithian) show low CIA values of 67–69, which suggests deposition in environments in which intense weathering was absent in the hinterland. The CIA values show an obvious degree of hydrolysis of alkaline cations because the vertical change in these values is correlated with Al_2O_3/Na_2O ratios. The ICV values show no correlation with the CIA values, which implies that the effect of selective removal and addition barely contributes to the change in these values. However, the CIA values and Al_2O_3/Na_2O ratios may be affected by the sediment grain size. The grain-size distribution in the selected samples shows no relationship to the CIA values and Al_2O_3/Na_2O ratios, with the exception of one sample from the topmost biocalcarenites. In addition, the average grain size of sample no. 83, which has a low CIA value, is similar to that of sample no. 86, which has a high CIA value. Thus, the CIA values are considered to reflect the degree of hydrolysis in the source area because the grain size change among these samples is not linked with either the CIA values or Al_2O_3/Na_2O ratios.

The A–CN–K ternary diagram indicates the weathering trend line (Fig. 8). The groups of the Triassic Tamba Kurkur Formation with Permian mudstones all plot along the same weathering trend line, which implies that they are derived from a common lithology.

Factors affecting chemical composition of sediments

The dominant controlling factors that affect the degree of paleoweathering are considered to be tectonic movements and climatic conditions in the source and depositional regions on land. Active tectonic forces, such as uplift of the hinterland, would sufficiently suppress chemical weathering by enhancing physical weathering and rapid accumulation. However, the lack of significant change in grain size and lithofacies indicates that there was no significant ongoing tectonic movement such as rapid uplift of the hinterland. Furthermore, a temporal decrease in the degree of paleoweathering is present from the upper part of the first mudstone interval to the second carbonate band with a return to the previous degree of paleoweathering in the third carbonate band.

Moreover, it is well known that relative sea level change affects the degree of chemical weathering. In particular, topographically flat regions on land, such as coastal plains and large flood plains, are strongly affected by relative sea level change (Cotton, 1963; Wright, 1970). In addition, the composition of sediments along the continental margin is controlled by relative sea level change with local modifications of topography occurring as a result of changes in the catchment area and sediment supply system (Curzi et al., 2006). Moreover, the change in the degree of mixing and reworking of initial sediments as a result of either a reduction or expansion in accommodation space due to topographical changes induced by sea level changes is a considerable factor to cause a compositional change of sediments (Strand, 1998; Muller, 2001).

In this study, the horizon showing a low degree of paleoweathering (shaded horizon in Fig. 7) is located at the transition into the first mudstone interval and second carbonate band. In this case, there is no relationship between lithology and the degree of paleoweathering. When carbonate deposition could be correlated with the transgressive or highstand stage of sea level change, it is considered that the horizon showing low paleoweathering degree has no connection to sea level change.

Implication of the horizon showing low paleoweathering degree

Climate conditions in the source area are important factors to control the degree of chemical weathering (Nesbitt and Young, 1982; Taylor and McLennan, 1985). In general, intensely weathered sediment tends to be provided from areas in a period in which wet, humid, and warm climates prevailed; in contrast, compositionally less mature sediment tends to be supplied by arid and cool periods (Prins and Postma, 2000; Tebbens and Veldkamp, 2000; Muller, 2001; Yang et al., 2002, 2008; Boulay *et al*., 2003; Curzi et al., 2006). Extended chemical weathering of flood plain deposits in humid subtropical climates can modify the initial sediment composition through reactions with groundwater (Singh, 2009). Even in mountainous regions, topographic changes leading to changes in sediment composition can be related to climate change (Yang et al., 2002).

Therefore, in the presented Manang section, the characteristic horizon showing a decrease in chemical weathering without substantial changes in the source rocks is likely to be closely linked to an abrupt change of weathering conditions such as climatic changes in the late Smithian. The Early Triassic climate was determined on the basis of paleoclimatic indicators, which generally suggest that in the Griesbachian interval, an extremely hot and uniform climate prevailed, whereas the Dienerian–Smithian period appears to have had steady and warm climatic conditions (Kidder and Worsley, 2004). Hermann et al. (2011, 2012) indicated a climate change from humid to dryer conditions around the Smithian–Spathian boundary in the Salt and Surghar Ranges in Pakistan and Tulong in Tibet. Moreover, Romano et al. (2013) reconstructed paleotemperature records on the basis of oxygen isotopes from fossil conodonts in the Salt Range, and they concluded that the middle–late Smithian was under extremely warm conditions. The chemical weathering data obtained here shows an abrupt decrease in the degree of weathering during the late Smithian. Conditions were more arid, indicating that this environmental change did not persist. These results imply that the climatic environment in the Early Triassic period on the northern margin of Gondwana was unstable.

Indications of climate change around the Smithian–Spathian period have been observed in several areas including the western Neo–Tethys (Bourquin *et al*., 2009) and Spitsbergen in

Norway (Galfetti *et al*., 2007b). An abrupt increase in immature siliciclastic materials during the Smithian period has been clearly recorded in a platform carbonate sequence of the western Paleo–Tethys (Stefani *et al*., 2010). Because climatic patterns are extremely complicated and vary in detail, several mechanisms could play a role in the local climate; therefore, there may be a disconnection between global and local climate regimes. In addition, the sampling interval was uneven in the second and third carbonate bands, and the duration of the dryer period remains undetermined. Thus, caution should still be maintained while extrapolating our results for the Triassic sequence in the Tethyan Himalayas to a global scale. The dispersed records of the Triassic climate should be combined near the northern Gondwana to Tethyan margins, though it is apparent that significant climate changes occurred in the late Smithian.

CONCLUSIONS

This study investigated the geochemistry of the Early Triassic mudstones in the Tethyan Himalayas in central Nepal. On the basis of lithofacies, the sediments are considered to have been deposited in offshore to hemiplegic environments. The chondrite normalized REE diagram for the Permian to Triassic mudstones suggests that the uniformity can be correlated to PAAS and a derivation from continental provenance. The paleoweathering index of the Early Triassic Griesbachian–early Smithian mudstones indicates a sediment supply from strongly weathered sources with CIA values of 76–81 (Nesbitt and Young, 1982). However, the mudstones in the late Smithian show weakly weathered sources with the CIA values of 68–74. The change in the degree of chemical weathering in this Lower Triassic sequence shows no dependence on lithology, grain size, or ICV values (Cox et al., 1995). This significant change in the degree of paleoweathering suggests an obvious change in the climatic conditions that caused continental weathering in the late Smithian. Although climatic patterns are extremely complicated, the observed abrupt decrease in continental weathering suggests a dryer condition and an unstable climatic environment in the Early Triassic period on the northern margin of Gondwana.

ACKNOWLEDGMENTS

We thank Prof. P. Gautam (Hokkaido Univ.) for offering advice on geology in the survey area, Dr. H. Machiyama for critical discussions and manuscript review, and Prof. Y. Miyake (Shinshu Univ., Japan) and Mr. T. Tsugane (Shinshu Univ.) for XRF measurements. We would also like to acknowledge Prof. M. Murayama (Kochi Univ.) for carbon isotope measurements and Mr. K. Otomo, Ms. A. Yamanaka, and Mr. K. Yukawa for assistance with the geological survey and sampling. Prof. E. Garzanti (Università Milano-Bicocca) is thanked for critical review of the manuscript. We are grateful to the Department of Geology and Mineralogy in Nepal for granting permission for fieldwork. This study is supported by Japan Society for Promotion of Science (No. 19403012). We are grateful to three anonymous reviewers for their constructive comments and valuable suggestions that significantly improved the initial paper.

REFERENCES

Atudorei, N.-V., Baud, A.,1997. Carbon isotope events during theTriassic. Albertiana 20,45-49.

Bassoullet, J.P., Colchen, M., 1977. La limite Permien-Trias dans le domaine tibetain de l'Himalaya du Nepal (Annapurnas-Ganesh Himal). In Jest, C., editor, Himalaya: Colloques internationaux du CNRS. Sevres-Paris, CNRS 268, 41-52.

Baud, A., Atudorei, V., Sharp, Z., 1996. Late Permian and Early Triassic evolution of the Northern Indian margin: carbon isotope and sequence stratigraphy. Geodinamica Acta. 9, 57–77.

Bordet, P., Colchen, M., Le Fort, P., 1975. Recherches geologiques dans l'Himalaya du Nepal, region du Nyi-Shang, Centre nationale de la recherche scientifique, Paris, 1-138.

Boulay, S., Colin, C., Trentesaux, A., Pluquet, F., Bertaux, J., Blamart, D., Buehring, C., Wang, P., 2003. Mineralogy and sedimentology of Pleistocene sediment in the South China Sea (ODP Site 1144). In Prell, W.L., Wang, P., Blum, P., Rea, D.K., Clemens, S.C. (Eds.), Proc. ODP, Sci. Results, 184: College Station, TX (Ocean Drilling Program), 1–21.

Bourquin, S., Guillocheau, F., Péron, S., 2009. Braided rivers within an arid alluvial plain (example from the lower Triassic, western German basin): Recognition criteria and expression of stratigraphic cycles: Sedimentology 56, 2235-2264.

Bourquin, S., Lopez Gomez, J., Bercovici, A., Diez, J. B., Broutin, J., Arche, A., Linol, B., Amour, F. 2011, The Permian–Triassic transition and the onset of Mesozoic sedimentation at the northwestern peri-Tethyan domain scale: Palaeogeographic maps and geodynamic implications. Palaeogeography, Palaeoclimatology, Palaeoecology, 299, 265-280.

Bodenhausen, J.W.A., De Booy, T., Egeler, C.G., Nijhuis, H.J., 1964, On the geology of central west Nepal - A preliminary note, Rep. 22nd Int. Geol. Congr. Delhi, XI, pp. 101-122.

Brayard, A., Bucher, H., Escarguel, G., Fluteau, F., Bourquin, S., Galfetti, T., 2006. The Early Triassic ammonoid recovery: paleoclimatic significance of diversity gradients: Palaeogeography, Palaeoclimatology, Palaeoecology 239, 374–395.

Brayard, A., Escarguel, G., Bucher, H., Monnet, C., Brühwiler, T., Goudemand, N., Galfetti, T., Guex, J., 2009. Good genes and good luck: ammonoid diversity and the end-Permian mass extinction: Science 325, 1118–1121.

Brühwiler, T; Goudemand, N; Galfetti, T; Bucher, H; Baud, A; Ware, D; Hermann, E; Hochuli, P A; Martini, R. 2009. The Lower Triassic sedimentary and carbon isotope records from Tulong (South Tibet) and their significance for Tethyan palaeoceanography. Sedimentary geology 222, 314-332.

Cullers, R.L., Barret, T, Carlson, R., Robinson, B., 1987. Rare earth element and mineralogical changes in Holocene soil and stream sediment: a case study in Wet Mountains, Colorado, U.S.A. Chemical Geology 63, 275-297.

Colchen, M. and Vachard, D., 1975, Nouvelles donnees sur la stratigraphie des terrains carboniferes et permiens du domaine tibetain de l' Himalaya du Nepal. C. Rend Acad. Sc. 281, 1963-1966, Paris.

Cotton, C.A., 1963. Levels of planation of marine beaches. Z. Geomorphology 7, 97–110.

Cox, R., Lowe D.R., Cullers, R.L., 1995. The influence of sediment recycling and basement composition on evolution of mudrock chemistry in the south-western United States: Geochimica Cosmochimica Acta 59, 2919-2940.

Curzi, P.V., Dinelli, E., Ricci Lucchi, M., Vaiani, S.C., 2006. Palaeoenvironmental control on sediment composition and provenance in the late Quaternary deltaic successions: a case study from the Po delta area (Northern Italy). Geological Journal 41, 591-612;

Dickins, J.M., 1993. Climate of the Late Devonian to Triassic. Palaeogeography, Palaeoclimatology, Palaeoecology 100, 89–94.

Eggins, S.M., Woodhead, J.D., Kinsley, L.P.J., Mortimer, G.E., Sylvester, P., McCulloch, M.T., Hergt, J.M., Handler, M.R., 1997. A simple method for the precise determination of 40 trace elements in geological samples by ICPMS using enriched isotope internal standardisation. Chemical Geology 134, 311-326.

Embry, A.F., 1997. Global sequence boundaries of the Triassic and their identification in the Western Canada Sedimentary Basin. Bulletin of Canadian Petroleum Geology 45 (4), 415–433.

Erwin, D.H., 1993. The Great Paleozoic Crisis: Life and Death in the Permian. Columbia Univ. Press, New York, 327p.

Fedo C.M., Young G.M., Nesbitt G.M., 1997. Paleoclimatic control on the composition of the Paleoproterozoic Serpent Formation, Huronian Supergroup, Canada: A greenhouse to icehouse transition: Precambrian Research 86, 201–223.

Fuchs, G., 1977. The geology of the Karnali and Dolpo regions, western Nepal. Jahrbuch Geologische Bundesanstalt 120, 165-217.

Fuchs, G., Widder, R.W., Tuladhar, R., 1988. Contributions to the geology of the Annapurna Range (Manang area, Nepal). Jahrbuch Geologische Bundesanstalt 131, 593-607.

Galfetti, T., Bucher,H., Brayard, A., Hochuli, P.A., Weissert, H., Guodun, K., Atudorei, V., Guex, J., 2007a. Late Early Triassic climate change: insights from carbonate carbon isotopes, sedimentary evolution and ammonoid paleobiogeography. Palaeogeography, Palaeoclimatology, Palaeoecology 243, 394–411.

Galfetti, T., Hochuli, P.A., Brayard, A., Bucher, H., Weissert, H., Vigran, J.O., 2007b. Smithian–Spathian boundary event: evidence for global climatic change in the wake of the end-Permian biotic crisis: Geology 35, 291–294.

Garzanti, E., 1999. Stratigraphy and sedimentary history of the Nepal Tethys Himalaya passive margin. Journal of Asian Earth Sciences 17, 805-827.

Garzanti, E., Nicora, A., Tintori, A., 1994a. Triassic stratigraphy and sedimentary evolution of the Annapurna Tethys Himalaya (Manang area, Central Nepal): Rivista Italiana di Paleontologia e Stratigrafia 100, 195-226.

Garzanti, E., Nicora, A., Tintori, A., Sciunnach, D., Angiolini, L., 1994b. Late Paleozoic stratigraphy and Petrography of the Thini Chu Group (Manang, central Nepal): Sedimentary record of Gondwana glaciation and rifting of Neotethys. Riv. It. Paleont. Strat., 100, 155-194.

Garzanti, E., Angiolini, L., Sciunnach, D., 1996. The Permian Kuling Group (Spiti, Lahaul and Zanskar; N.W. Himalaya): sedimentary evolution during rift/drift transition and initial opening of Neotethys. Riv. It. Paleont Strat 102, 175-200.

Garzanti, E., Nicora, A. , Rettori, R., 1998. Permo-Triassic boundary and Lower to Middle Triassic in South Tibet. Journal of Asian Earth Sciences 16, 143-157.

Gianolla, P., Jacquin, T., 1998. Triassic sequence stratigraphic framework of western European basins. In: de Graciansky, P.-C., Hardenbol, J., Jacquin, T., Vail, P.R. (Eds.), Mesozoic and Cenozoic Sequence Stratigraphy of European Basins: SEPM Special Publication, 60, pp. 643–650. Tulsa SEPM (Society for Sedimentary Geology).

Golonka, J., Ford, D., 2000. Pangean (Late Carboniferous–Middle Jurassic) paleoenvironment and lithofacies. Palaeogeography, Palaeoclimatology, Palaeoecology 161, 1–34.

Goudemand, N., Orchard, M.J., Bucher, H., Jenks, J., 2012. The elusive origin of *Chiosella timorensis* (Conodont Triassic). Geobios 45, 199-207.

Hallam, A., 1991. Why was there a delayed radiation after the end-Permian mass extinction?: Historical Biology 5, 257–262.

Hallam, A., Wignall, P.B., 1997. Mass Extinctions and Their Aftermath: Oxford University Press, Oxford, 328 p.

Haq, B.U., Shutter, S.R., 2008. A chronology of Paleozoic sea-level change4s. Science 322, 64-68.

Haq, B.U., Hardenbol, J., Vail, P.R., 1988. Mesozoic and Cenozoic chronostratigraphy and cycles of sea-level change. In: Wilgus, C.K., Hastings, B.S., Kendall, C.G.St.C., Posamentier, H.W., Ross, C.A., Van Wagoner, J.C. (Eds.), Sea-Level Changes: An Integrated Approach. : Special Publication, No. 42. Society of Economic Paleontologists and Mineralogists, Tulsa, Oklahoma, pp. 71–108

Hardenbol, J., Thierry, J., Farley, M.B., Jacquin, T., de Graciansky, P.C., Vail, P., 1998. Mesozoic and Cenozoic sequence chronostratigraphic framework of European basins. In Graciansky, P.C. et al. (eds.), Mesozoic and Cenozoic Sequence Stratigraphy of European Basins, SEPM Special Publication 60, 3-13.

Hatleberg, E.W., Clark, D.L., 1984. Lower Triassic conodonts and biofacies interpretations: Nepal and Svalbard. Geol. Paleont 18, 101-112.

Hermann, E., Hochuli, P.A., Mehay, S., Bucher, H., Brühwiler, T., Ware, D., Hautmann, M., Roohi, G., ur-Rehman, K., Yaseen, A., 2011. Organic matter and palaeoenvironmental signals during the Early Triassic biotic recovery: The Salt Range and Surghar Range records. Sedimentary Geology 234, 19-41.

Hermann, E., Hochuli, P.A., Bucher, H., Brühwiler, T., Hautmann, M., Ware, D., Weissert, H., Roohi, G., Yaseen, A., Khalil-ur-Rehman, 2012. Climatic oscillations at the onset of the

Mesozoic inferred from palynological records from the North Indian Margin. Journal of the Geological Society 169, 227-237.

Knoll, A.H., Bambach, R.K., Payne, J.L., Pruss, S., Fischer, W.W., 2007. Paleophysiology and end-Permian mass extinction: Earth and Planetary Science Letters 256, 295–313.

Kidder, D.L., Worsley, T.R., 2004. Causes and consequences of extreme Permo–Triassic warming to globally equable climate and relation to Permo–Triassic extinction and recovery: Palaeogeography, Palaeoclimatology, Palaeoecology 203, 207–237.

Kiehl, J.T., Shields, C.A., 2005. Climate simulation of the latest Permian: implications for mass extinction: Geology. 33, 757–760.

Looy, C.V., Brugman, W.A., Dilcher, D.L., Visscher, H., 1999. The delayed resurgence of equatorial forests after the Permian–Triassic ecologic crisis: PNAS 96, 13857–13862.

McLennan, S.M., Taylor, S.R., Eriksson, K.A., 1983. Geochemistry of Archean shales from the Pilbara Supergroup, Western Australia. Geochimica Cosmochimica. Acta 47, 1211-1222.

Marshall, J.D., 1992. Climatic and oceanographic isotopic signals from the carbonate rock record and their preservation. Geological Magazine 129, 143-160.

Muller, A., 2001. Late- and Postglacial Sea-Level Change and Paleoenvironments in the Oder Estuary, Southern Baltic Sea. Quaternary Research 55, 86–96.

Miyake, Y., Tsugane, T., Kanai, T., Ikemoto, M., 1996. X-ray fluorescence analysis of major elements in silicate rocks : prepration of glass bead pellets of a high ratio of sample to flux and the accuracy of the rapid analysis, J. Fac. Sci. Shinshu Univ. 31, 105-117. (Japanese with English abstract)

Nesbitt, H.W., Young, G.M., 1982. Early Proterozoic climates and plate motions inferred from major element chemistry of lutites: Nature 299, 715–717.

Nesbitt H.W., Young G.M., 1984. Prediction of some weathering trends of plutonic and volcanic rocks based on thermodynamic and kinetic considerations: Geochimica et Cosmochimica Acta 48, 1523–1534.

Nicora, A., Garzanti, E., 1997. The Permian/Triassic boundary in the central Himalaya. Albertiana 19, 47-51.

Nicora, A., Garzanti, E., Tintori, A., 1992. Early Triassic of the Nepal Tethys Himalaya: stratigraphy and sedimentary evolution, 62-63, VIII Himalaya-Tibet-Karakorum Workshop, Vienna.

Orchard, M.J., 2007. Conodont diversity and evolution through the latest Permian and Early Triassic upheavals: Palaeogeography, Palaeoclimatology, Palaeoecology. 252, 93–117.

Payne, J., Turchyn, A., Paytan, A., Depaolo, D., Lehrmann, D., Yu, M.; Wei, J., 2010. Calcium isotope constraints on the end-Permian mass extinction: Proceedings of the National Academy of Sciences of the United States of America 107, 8543–8548.

Potter, P.E., Maynard, J.B., Depetris, P.J., 2005. Chapter 7, Provenance of Mudstones. In Mud and Mudstones, 157-174, Springer, 297p.

Prins, M.A. Postma, G., 2000. Effects of climate, sea level, and tectonics unraveled for last deglaciation turbidite records of the Arabian Sea. Geology 28, 375-378.

Raup, D.M., Sepkoski, J.J., 1982. Mass extinctions in the marine fossil record: Science 215, 1501–1503.

Retallack, G.J., 2005. Earliest Triassic Claystone Breccias and Soil-Erosion Crisis: Journal of Sedimentary Research 75, 679-695.

Romano, C., Goudemand,N., Vennemann, T.W., Ware, D., Schneebeli-Hermann, E., Hochuli, P.A., Brühwiler, T., Brinkmann, W., Bucher, H., 2013. Climatic and biotic upheavals following the end-Permian mass extinction. Nature geoscience 6, 57-60.

Roser, B., Kimura, J. and Hisatomi, K., 2000. Whole-rock elemental abundances in sandstones and mudrocks from the Tanabe Group, Kii Penisula, Japan. Geosciences Reptort of the Shimane University 19, 101-112.

Skjold, L.J., van Veen, P.M., Kristensen, S.-E., Rasmussen, A.R., 1998. Triassic sequence stratigraphy of the southwestern Barents Sea. In: de Graciansky, P.-C., Hardenbol, J., Jacquin, T., Vail, P.R. (Eds.), Mesozoic and Cenozoic Sequence Stratigraphy of European Basins: SEPM Special Publication, 60, pp. 651–666. Tulsa SEPM (Society for Sedimentary Geology).

Senowbari-Daryan, B., Zühlke, R., Bechstädt, T., Flügel, E., 1993. Anisian (Middle Triassic) Buildups of the Northern Dolomites (Italy): the recovery of reef communities after the Perm/Triassic crisis: Facies 28, 181–256.

Singh, P., 2009. Major, trace and REE geochemistry of the Ganga River sediments: Influence of provenance and sedimentary processes. Chemical Geology 266, 242-255.

Stefani, M.,, Furin, S., Gianolla, P., 2010. The changing climate framework and depositional dynamics of the Triassic carbonate platforms from the Dolomites, Palaeogeography, Palaeoclimatology, Palaeoecology 290, 43–57.

Strand, K., 1998. Sedimentary facies and sediment composition changes in response to tectonics of the Côte d'Ivoire-Ghana transform margin. In Mascle, J., Lohmann, G.P., Moullade, M. (Eds.), Proc. ODP, Sci. Results, 159: College Station, TX (Ocean Drilling Program), 113–123.

Taylor, S. R., McLennan, S. M., 1985. The Continental Crust: Its Composition and Evolution, Blackwell, Oxford, 328 p.

Tebbens, L.A. Veldkamp, 2000. Late Quaternary evolution of fluvial sediment composition: a modeling case study of the River Meuse. Global and Planetary Change 27, 187-206.

von Rad, U., DuÈ rr, S.B., Ogg, J.G., Wiedmann, J., 1994. The Triassic of the Thakkhola (Nepal). I: stratigraphy and paleoenvironment of a north-east Gondwana rifted margin. Geol. Rundsch 83, 76-106.

Waterhouse, J.B., 1977. The Permian rocks and fauna from Dolpo, North-west Nepal. Coll. Int. C.N.R.S. Paris 268, 479-496.

Waterhouse, J.B., 1994. The Early and Middle Triassic ammonoid succession of the Himalayas in western and central Nepal - Part 1. Stratigraphy, classification and Early Schytian ammonoid systematics. Paleontographica, Abt. A 232, 1-83.

Waterhouse, J.B., 2010, Lopingian (Late Permian) stratigraphy of the Salt Range, Pakistan and Himalayan region. Geol.J., 45, 264-284.

Wignall, P.B., Twitchett, R.J., 2002. Permian–Triassic sedimentology of Jameson Land, East Greenland: incised submarine channels in an anoxic basin: Journal of the Geological Society London 159, 691–703.

Wright, L.W., 1970. Variations in the level of the cliff/shore platform junction along the south coast of Great Britain. Marine Geology 9, 347–353.

Wronkiewicz, D. J. and Condie, K. C., 1990. Geochemistry and mineralogy of sediments from the Ventersdorp and Transvaal Supergroups, South Africa: cratonic evolution during the early Proterozoic. Geochim. Cosmochim. Acta 54, 343–354.

Yang, X.P., Zhu, Z.D., Jaekelc, D., Owend, L.A., Han, J.M., 2002. Late Quaternary palaeoenvironment change and landscape evolution along the Keriya River, Xinjiang, China: the relationship between high mountain glaciation and landscape evolution in foreland desert regions. Quaternary International 97-98, 155-166.

Worsley, T. R., Moore, T. L., Fraticelli, C. M., and Scotese, C. R., 1994. Phanerozoic CO2 levels and global temperatures inferred from changing paleogeography, in Klein, G. de V.,ed., Pangea: Paleoclimate, tectonics and sedimentation during accretion, zenith and breakup of a supercontinent: Geological Society of America Special Paper 288, p. 57–74.

FIGURE CAPTIONS

Fig. 1 A: Simplified geological map of the Himalayan area; B: Index map of the sample section in the Manang area, Tethyan Himalayas; C: $\delta^{13}C_{carb}$ record from the Tamba Kurkur Formation in the Manang area and the correlation with the Tulong area in South Tibet (Brühwiler et al., 2009) and the Losar area, Spiti, India (Galfetti et al., 2007a). Horizons A–C (shaded horizons) indicate correlatable remarkable isotope excursions. Horizons yielding conodonts after Garzanti *et al*. (1994) are indicated by sequence 1–7; see regional geology section in text. Abbreviations: G.: Griesbachian; D.: Dienerian; HST: highstand system tract; TST: transgressive system tract; LST: lowstand system tract; SB: system boundary.

Fig. 2 Photographs and photomicrographs. A: Outcrop of the sample section. Abbreviations: P:Permian Puchenpra Formation; TB: topmost biocalcarenites; Tc1, Tc2, and Tc3: first, second, and third carbonate bands of the Tamba Kurkur Formation, respectively; M:

Mukut Formation. B: Cross-bedded sandstone in the Puchenpra Formation. C: Contact of the Puchenpra Formation, topmost biocalcarenites, and first carbonate band of the Tamba Kurkur Formation. Note the undulated boundary between the Puchenpra Formation and topmost biocalcarenites. D: Echinoidal wackestone–packstone including quartz grains in the topmost biocalcarenites. E: Mudstone containing thinly-bedded, alternating layers of red–purple and black mudstones in the first mudstone interval. F: Small burrow on the bedding plane of the red–purple mudstone in the first mudstone interval. G: Grading structure in the red–purple mudstone in the first mudstone interval. The arrow indicates fining trend of grain size. H: Biomicritic wackestone including small ammonoid (A), thin-shelled bivalve (B), and ostracoda (O?) in the first carbonate band. I: Biomicritic packstone–wackestone with thin-shelled bivalves in the second carbonate band. J: Biomicritic wackestone–packstone, containing fragments of small bivalves in the third carbonate band. K: Nodular limestone in the third carbonate band. Note the intensely deformed structure by tectonic–diagenetic brecciation with dissolution seams (dark color). L: Alternation of marly limestone and mudstone in the Mukut Formation.

Fig. 3 Thin-section photomicrograph of mudstones in the Triassic Tamba Kurkur Formation in the Manang area, central Nepal. a: Sample no. 66 from the first mudstone interval, b: sample no. 75 from the first mudstone interval, c: sample no. 82 from the second carbonate band, 4: sample no. 85 from the second carbonate interval. The white triangles indicate quart and feldspar grains in mudstone. All photomicrographs were taken under open polarized light.

Fig. 4 Variation of $\delta^{13}C_{carb}$–$\delta^{18}O_{carb}$ for the carbonate in the Triassic topmost biocalcarenites, Tamba Kurkur, and Mukut Formations in the Manang area, central Nepal.

Fig. 5 Variation of major elements against SiO_2 for the mudstones in the Permian Puchenpra, Triassic topmost biocalcarenites, Tamba Kurkur, and Mukut Formations in the Manang area, central Nepal.

Fig. 6 Chondrite-normalized spider diagram of average REE abundances in the Permian and Triassic mudstones from the Manang area, central Nepal compared with the PAAS value (Taylor and McLennan, 1985). Note that all mudstones in the Tamba Kurkur Formation have a similar source that correlates in composition to felsic igneous rock.

Fig. 7 Vertical variation of CIA (Nesbitt and Young, 1982), Al_2O_3/Na_2O ratios, and ICV (Cox et al., 1995) within the stratigraphic column. Note the visible decrease in CIA and Al_2O_3/Na_2O values in the second carbonate band (shaded horizon; middle Smithian). The hatched region in the CIA and Al_2O_3/Na_2O diagram represents the variation of CIA values in average shales (Taylor and McLennan, 1985). The results of grain size analysis for mudstone are also shown.

Fig. 8 A–CN–K plots (Nesbitt and Young, 1984) for mudstone samples in the Permian Puchenpra, Triassic topmost biocalcarenites, Tamba Kurkur, and Mukut Formations in the Manang area, central Nepal. A: Al_2O_3, CN: $CaO + Na_2O$, K: K_2O.

Supplemental Table 1. REE data from the Triassic, Manang area, central Nepal.

Supplemental Table 2. Major geochemistry, CIA, Al_2O_3/ Na_2O, and ICV data from the Triassic, Manang area, central Nepal.

Appendix

METHODOLOGY

In this study, analytical methods were primarily used to determine the bulk chemical composition of major and REEs for 50 mudstone samples. The major element measurements were obtained by X-ray fluorescence (XRF). For the REE composition, samples were analyzed by inductively coupled plasma mass spectrometry (ICP-MS). To estimate the geochemical effects of grain-size variation, the distributions of grain size in mudstones were obtained through thin-section examinations.

Geochemistry: To determine the mudstone bulk chemistry, samples were carefully collected from the mudstone layers of the Puchenpra, topmost biocalcarenites, Tamba Kurkur, and Mukut Formations. The stratigraphic intervals for sampling ranged from 0.3 to 5 m along the section. Thin sections were prepared from all mudstone samples. Other parts of the samples were crushed and ground to a fine powder with a steel and agate mortar, and precautions were taken to avoid contamination of the samples. The samples were kept at a constant particle size to avoid the risk of variation in fluorescence intensities. Conventional fused glass disks were favored for the measurement of major elements because the decomposition of a portion of the sample and flux can produce a homogeneous glass, thus eliminating the effects of particle size and mineralogy. The fused glass disks were composed of a 1:2 mixture of powdered dry sample and $Li_2B_4O_7$ flux, respectively. After being properly mixed, they were heated in Pt crucibles by using an electric heating system. During fusion, the melt was agitated to produce a homogeneous glass. For major element analysis, the compositions of all samples were measured by an automatic XRF spectrometer (Phillips PW2400) at the Faculty of Science, Shinshu University, Japan, using established procedures and detection limits (Miyake et al., 1996).

To clarify the nature of the mudstones, average abundances of REE were examined. Nine samples from the first mudstone interval, four samples from the second carbonate band, one sample from the third carbonate band, and three samples from the Mukut Formation were selected and analyzed. REE analysis was performed following the procedure established by Roser et al. (2000) with the variation of dissolving fluxed samples in concentrated nitric acid rather than perchloric acid. Sample powders were dissolved in concentrated HF–HNO_3 by using Pt crucibles and were then evaporated. Following this step, Na_2CO_3 alkali flux was added, and the sample was heated in an electric furnace. The fluxed samples were dissolved in concentrated HNO_3, HCl, and ultrapure water. The samples were finally diluted 20,000 times. For calibration, we used reference values from BHVO-1 (basalt; Hawaii, U.S. Geological Survey [USGS]; Eggins et al., 1997). REE abundances were analyzed by using an inductively coupled plasma mass spectrometer (Agilent 7500a) at the Faculty of Science, Niigata University, Japan. The average REE abundances were calculated and are shown as chondrite normalized values in Fig. 6.

For the estimation of the geochemical characteristics of the degree of weathering at the time of deposition, we calculated the chemical index of alteration (CIA) from the major element geochemistry (Nesbitt and Young, 1982; Fedo et al., 1997). CIA is expressed as CIA = molar $[(Al_2O_3)/(Al_2O_3 + CaO^* + Na_2O + K_2O)] \times 100$, where CaO* represents CaO in silicate minerals only. The Al_2O_3/Na_2O ratio is directly calculated from Al_2O_3 wt% and Na_2O wt% obtained from the XRF results. The index of compositional variability (ICV) value, which is expressed as ICV $= [Fe_2O_3 + K_2O + Na_2O + CaO + MgO + MnO + TiO_2]/Al_2O_3$ (Cox et al., 1995), indicates the degree of maturity of the fine alumino–siliciclastic material delivered to the sedimentary basin.

Carbon isotope analysis: Sampling of limestone and marlstone for carbon isotope measurements was conducted at intervals ranging from 0.3 to 5 m along the sample section.

Powders were produced from samples by using a diamond cutter, and hand specimens were carefully examined to avoid cracks, veins, and weathering features. Fifty-six samples were analyzed by using an automated carbonate preparation system (carbonate device) connected to the Thermo-Finnigam MAT253 mass spectrometer at the Kochi Core Center in Kochi University, Japan. Reproducibility of replicate analyses was better than ±0.03‰ for standards and ±0.2‰ for sediment samples of both carbon isotope values. All isotope results are defined as per mill (‰) deviation vs. PDB and were calibrated to NBS-19 international standards.

Grain-size analysis: Grain-size analysis was conducted by thin-section examination of seven selected mudstone samples by using an eye-piece micrometer to measure the dimensions of quartz and feldspar grains under a standard petrographic microscope of 400× magnification. Random grains were selected by using a mechanical stage with a grid spacing of 0.2 mm.

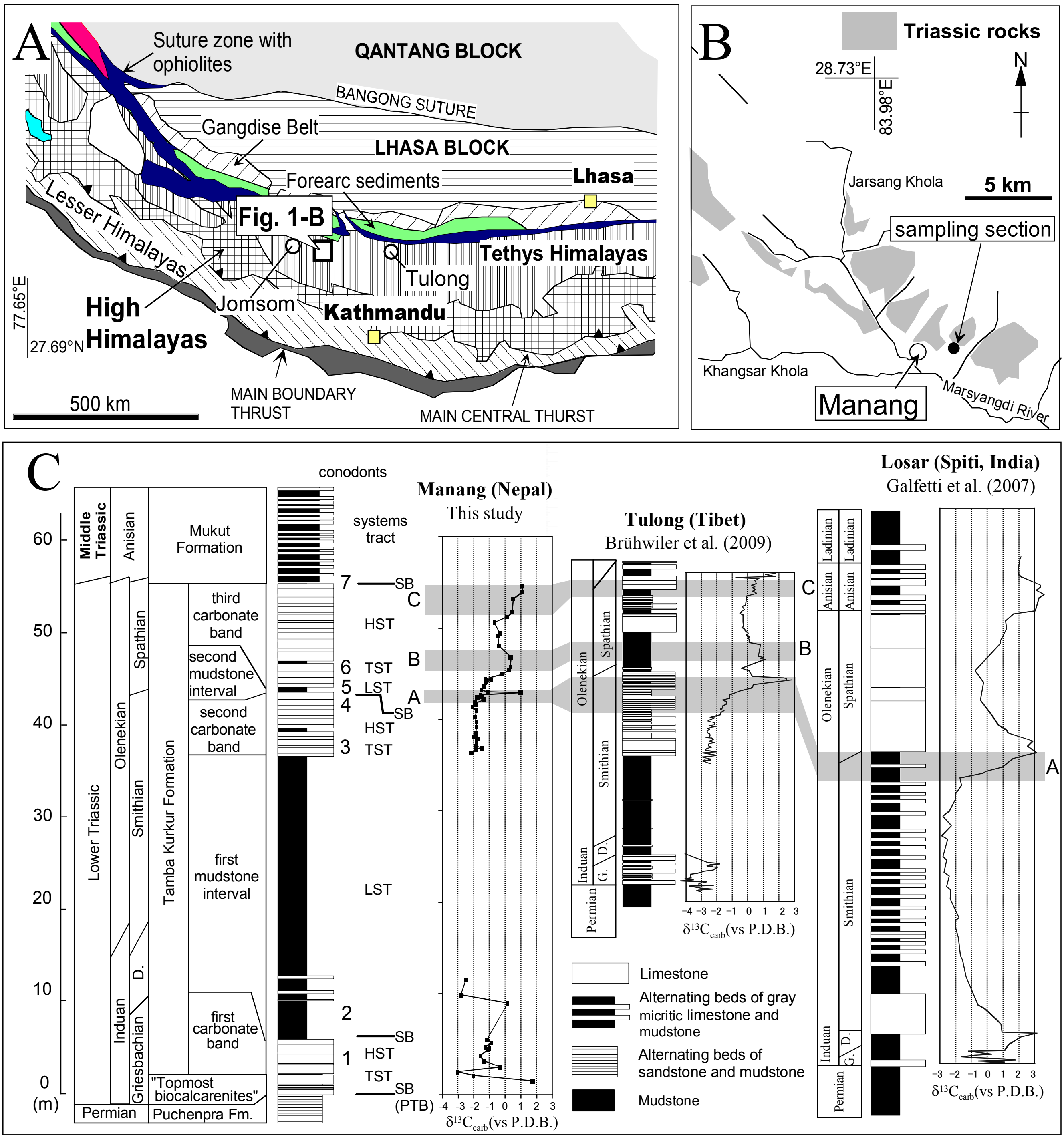

Fig. 1 Yoshida et al.

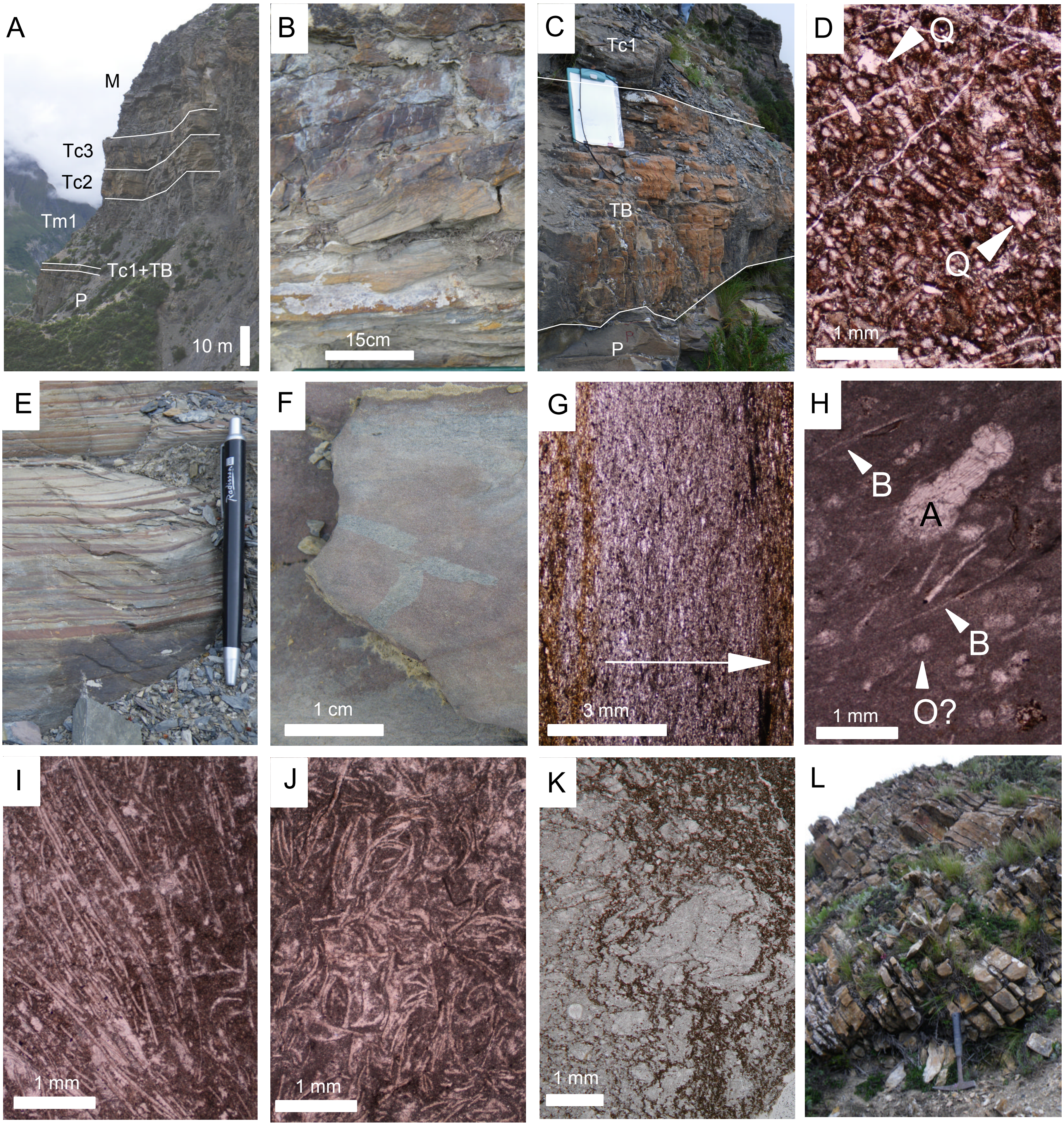

Fig. 2 Yoshida et al.

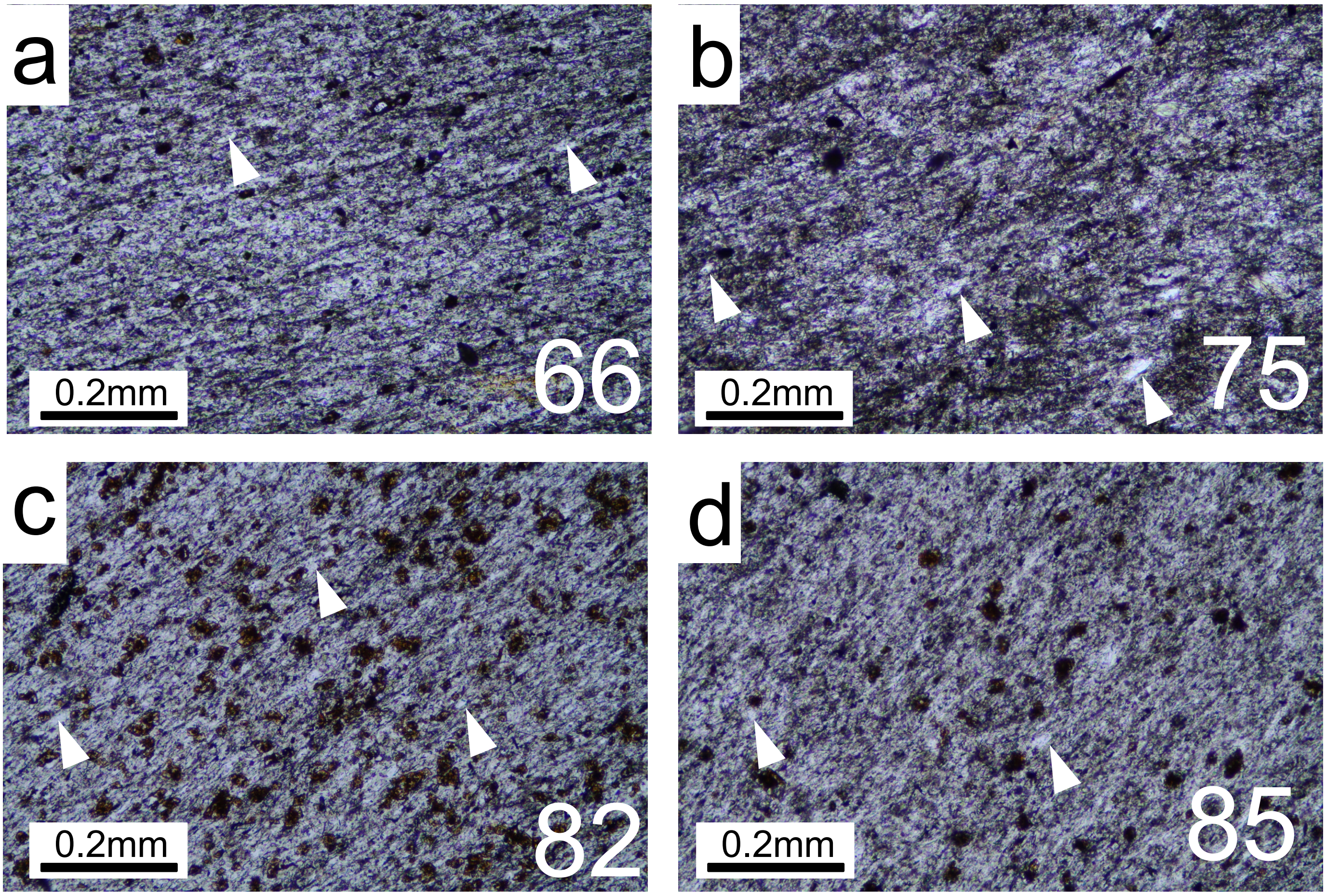

Fig. 3 Yoshida et al.

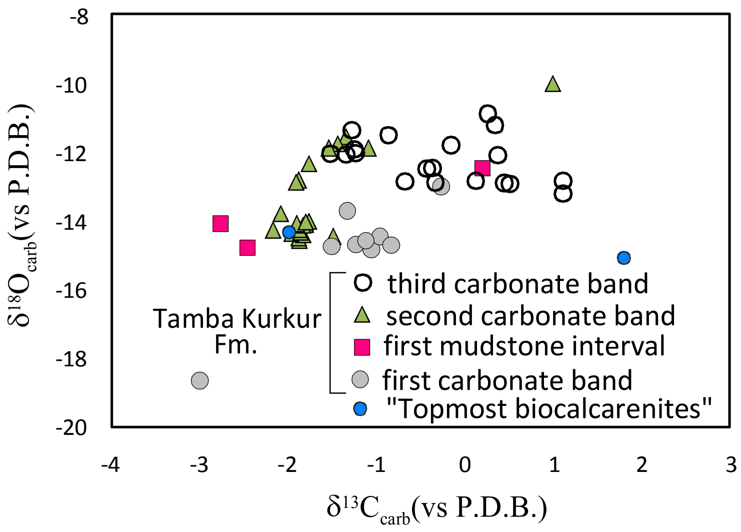

Fig. 4 Yoshida et al.

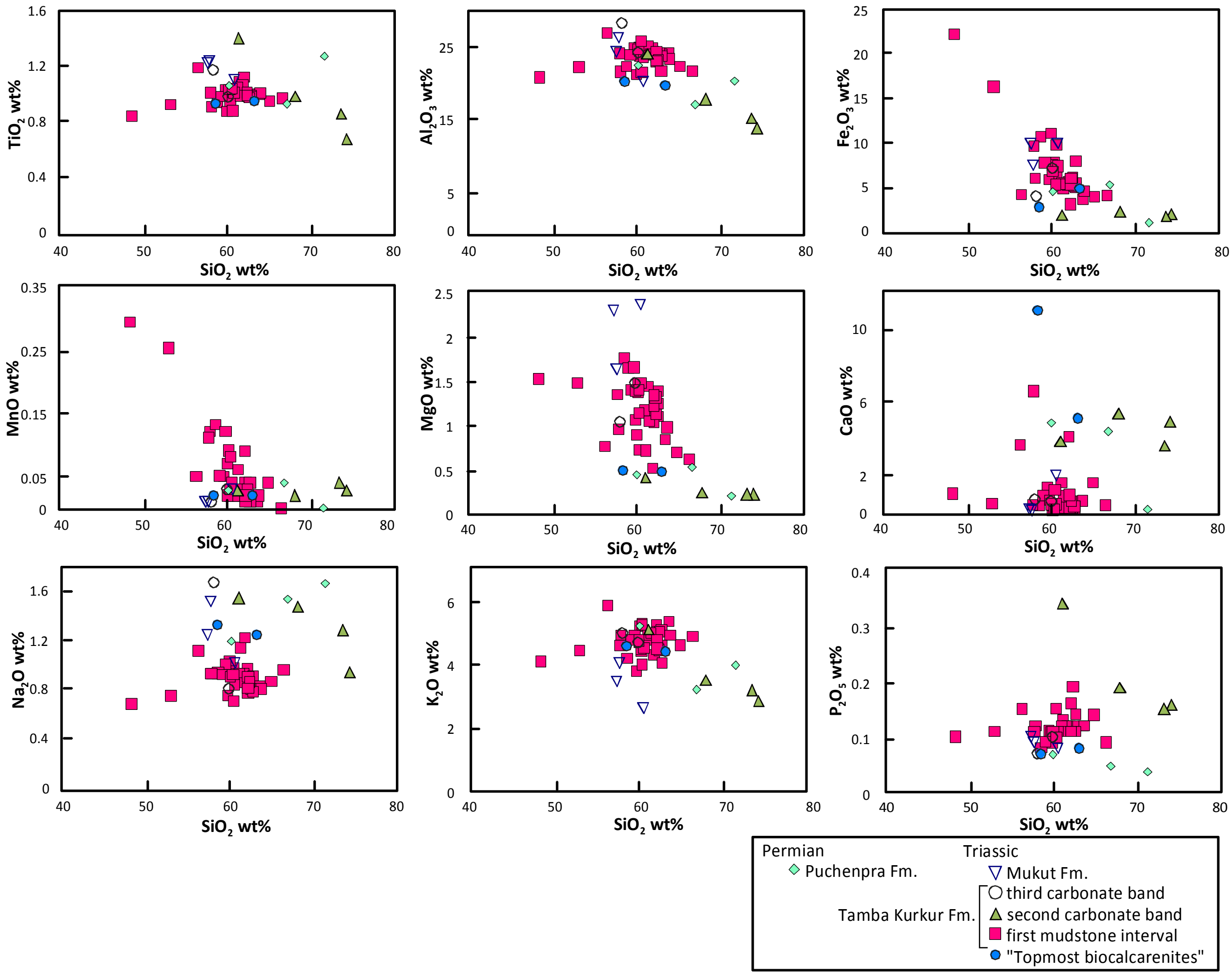

Fig. 5 Yoshida et al.

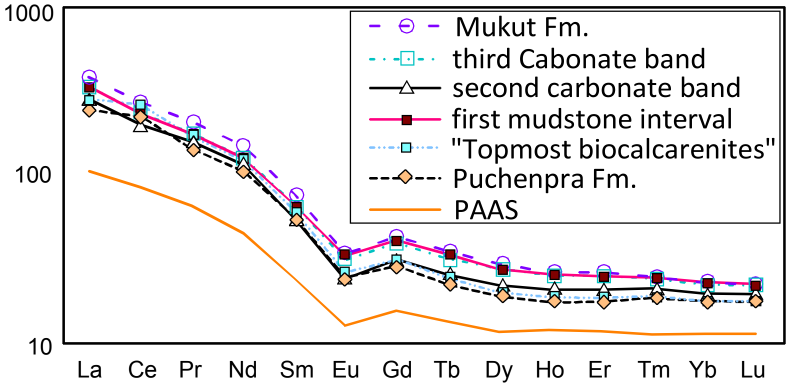

Fig. 6 Yoshida et al.

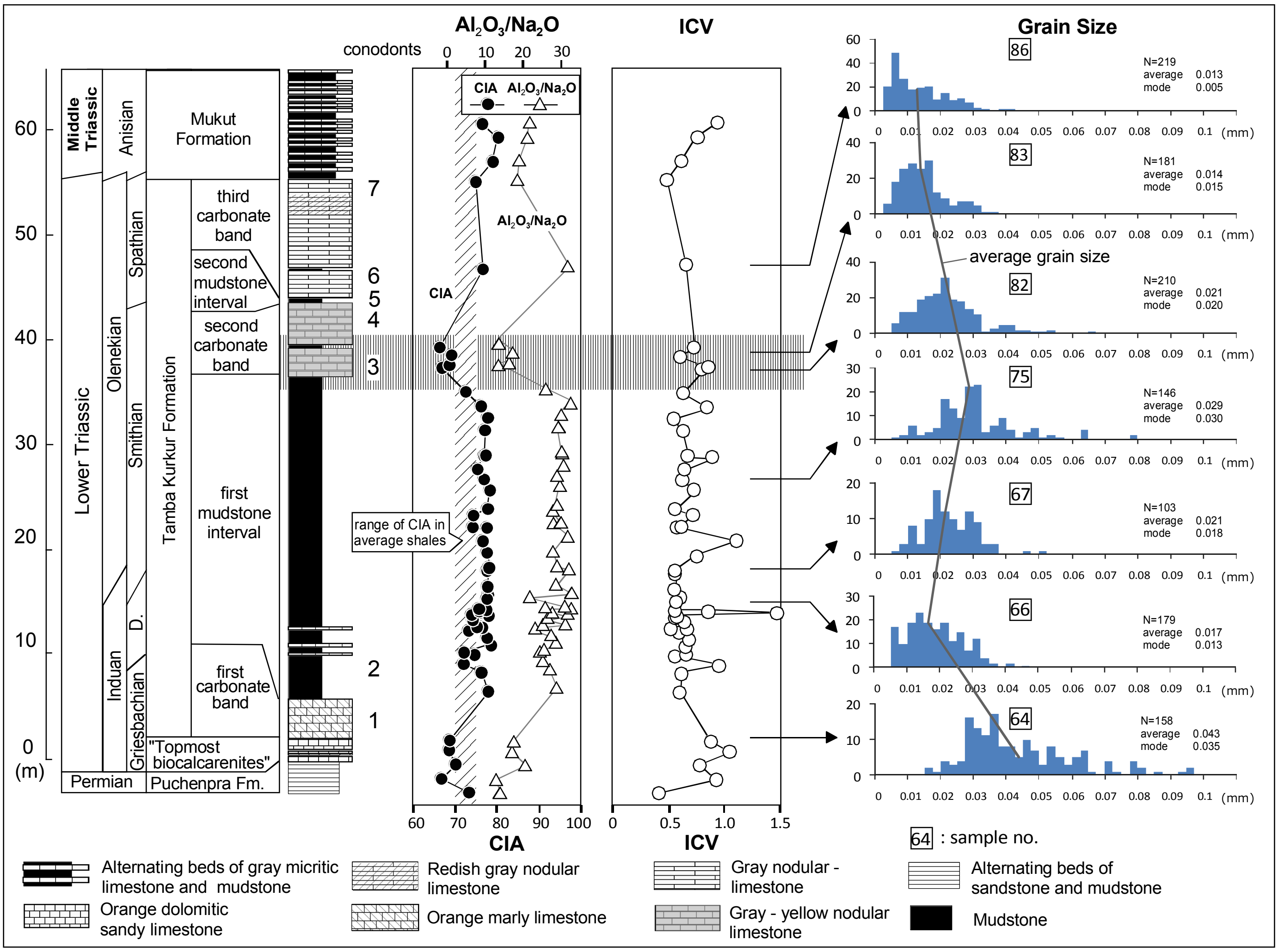

Fig. 7 Yoshida et al.

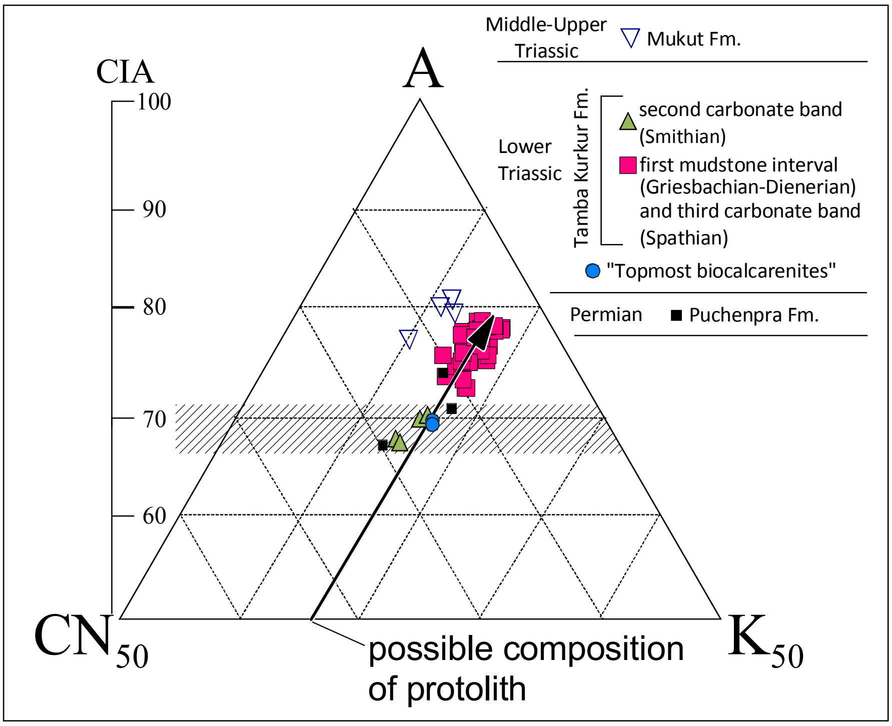

Fig. 8 Yoshida et al.

Supplemental table 1
REE data from the Permian-Triassic sediments, Manang area, central Nepal.

	Puchenpra Fm.	Topmost bio-calcarenites	Tamba Kurkur Fm.			Mukut Fm.	PAAS
			First mudstone interval	Second carbonate band	Third carbonate band		
La(N)	243.6	280.6	329.3	283.4	337.2	377.7	103.5
Ce(N)	216.0	258.8	232.1	197.9	232.8	268.9	83.6
Pr(N)	141.9	166.7	177.3	155.6	175.9	204.9	65.0
Nd(N)	106.2	122.0	127.7	112.6	125.7	147.5	45.0
Sm(N)	57.2	61.1	66.9	55.2	66.1	77.0	24.2
Eu(N)	24.8	25.7	32.5	24.2	30.5	33.5	12.6
Gd(N)	28.4	30.7	40.0	31.4	38.4	42.6	15.4
Tb(N)	22.2	24.2	33.6	25.4	31.4	34.7	13.3
Dy(N)	18.8	20.0	28.6	22.2	27.2	29.0	11.5
Ho(N)	17.5	18.6	25.8	20.7	25.2	26.8	11.8
Er(N)	17.3	18.4	25.6	21.0	24.8	25.7	11.6
Tm(N)	18.3	18.6	24.9	21.0	23.8	24.3	11.2
Yb(N)	17.7	17.4	22.8	19.5	22.2	22.3	11.3
Lu(N)	17.6	17.3	22.5	19.6	21.8	21.6	11.3
(La/Yb)N	13.8	16.2	14.5	14.6	15.2	16.9	9.2
(La/Sm)N	4.3	4.6	4.9	5.1	5.1	4.9	4.3
(Gd/Yb)N	1.6	1.8	1.8	1.6	1.7	1.9	1.4

Note: (N) indicates chondrite normalized value.

Supplemental table 2
Major bulk rock geochemistry, CIA, Al_2O_3/ Na_2O and ICV data from the Permian - Triassic sediments, Manang area, central Nepal.

Sample name	Sampling horizon (m)	System	Formation	Stratigraphic division	SiO_2	TiO_2	Al_2O_3	Fe_2O_3	MnO	MgO	CaO	Na_2O	K_2O	P_2O_5	Total	CIA	Al_2O_3/Na_2O	ICV
60	−3	Permian	Puchenpra Fm.		71.54	1.28	20.22	0.82	0.00	0.21	0.21	1.66	4.02	0.04	100.00	73.29	12.18	0.41
61	−1.7	Permian	Puchenpra Fm.		66.98	0.92	17.16	5.15	0.04	0.55	4.39	1.53	3.25	0.05	100.00	66.78	11.24	0.92
62	-0.3	Permian	Puchenpra Fm.		60.22	1.05	22.47	4.35	0.03	0.45	4.91	1.19	5.26	0.07	100.00	70.02	18.81	0.77
63	1	Lower Triassic	"Topmost biocalcarenites"		58.58	0.93	20.33	2.72	0.02	0.50	10.95	1.32	4.58	0.07	100.00	68.58	15.37	1.03
64	2	Lower Triassic	"Topmost biocalcarenites"		63.23	0.95	19.59	4.80	0.02	0.49	5.15	1.23	4.46	0.08	100.00	68.78	15.87	0.87
M2	7.2	Lower Triassic	Tamba Kurkur Fm.	First mudstone interval	60.36	0.93	24.86	6.53	0.09	0.89	0.10	0.92	5.22	0.10	100.00	77.76	26.91	0.59
0826M3	9	Lower Triassic	Tamba Kurkur Fm.	First mudstone interval	60.60	1.01	24.43	6.41	0.02	0.72	0.41	0.97	5.28	0.15	100.00	76.08	25.31	0.61
M4	9.8	Lower Triassic	Tamba Kurkur Fm.	First mudstone interval	58.10	0.90	21.51	5.86	0.12	0.96	6.58	0.92	4.94	0.12	100.00	71.98	23.40	0.94
0826M5	10.7	Lower Triassic	Tamba Kurkur Fm.	First mudstone interval	66.62	0.96	21.60	3.89	0.00	0.62	0.37	0.95	4.90	0.09	100.00	74.65	22.69	0.54
M6	10.9	Lower Triassic	Tamba Kurkur Fm.	First mudstone interval	62.28	0.98	22.77	2.93	0.09	0.52	4.09	0.96	5.26	0.12	100.00	72.01	23.74	0.65
0826M7	11.6	Lower Triassic	Tamba Kurkur Fm.	First mudstone interval	60.51	1.02	24.04	7.17	0.02	1.48	0.31	0.90	4.44	0.10	100.00	78.43	26.81	0.64
0826M8	12.3	Lower Triassic	Tamba Kurkur Fm.	First mudstone interval	60.46	1.03	23.60	7.61	0.02	1.37	0.39	0.92	4.50	0.10	100.00	77.50	25.53	0.67
65	13	Lower Triassic	Tamba Kurkur Fm.	First mudstone interval	61.44	1.08	24.29	4.73	0.06	0.72	1.61	1.13	4.80	0.13	100.00	73.13	21.45	0.58
MA−1(blk)	13.3	Lower Triassic	Tamba Kurkur Fm.	First mudstone interval	60.18	1.01	24.01	7.37	0.07	1.06	0.47	1.02	4.71	0.09	100.00	76.42	23.48	0.65
M9	13.35	Lower Triassic	Tamba Kurkur Fm.	First mudstone interval	63.77	0.99	23.98	3.52	0.01	0.84	0.59	0.82	5.37	0.12	100.00	75.15	29.30	0.51
MA−2(blk)	14	Lower Triassic	Tamba Kurkur Fm.	First mudstone interval	59.74	1.02	24.65	5.76	0.05	1.41	1.33	1.00	4.93	0.11	100.00	74.09	24.69	0.63
0826M10	14.4	Lower Triassic	Tamba Kurkur Fm.	First mudstone interval	62.91	0.99	23.92	4.89	0.01	1.10	0.14	0.80	5.11	0.12	100.00	77.83	29.97	0.54
66	14.5	Lower Triassic	Tamba Kurkur Fm.	First mudstone interval	65.12	0.94	22.20	3.77	0.04	0.70	1.62	0.86	4.62	0.14	100.00	73.92	25.86	0.56
0826M11A	14.9	Lower Triassic	Tamba Kurkur Fm.	First mudstone interval	48.54	0.83	20.73	22.18	0.30	1.53	1.01	0.67	4.11	0.10	100.00	75.68	30.86	1.46
MA−3(blk)	15	Lower Triassic	Tamba Kurkur Fm.	First mudstone interval	58.79	0.94	22.23	10.59	0.13	1.76	0.35	0.93	4.20	0.08	100.00	77.35	24.00	0.84
0826M11B	15.1	Lower Triassic	Tamba Kurkur Fm.	First mudstone interval	63.95	1.00	23.19	4.39	0.02	0.98	0.62	0.80	4.93	0.12	100.00	75.59	29.13	0.55
0826M12	16.4	Lower Triassic	Tamba Kurkur Fm.	First mudstone interval	62.38	0.97	23.51	5.85	0.04	1.03	0.24	0.76	5.05	0.16	100.00	77.65	30.93	0.59
67	16	Lower Triassic	Tamba Kurkur Fm.	First mudstone interval	62.00	1.11	24.26	5.40	0.02	1.17	0.37	1.21	4.32	0.12	100.00	77.44	19.98	0.56
68	17.2	Lower Triassic	Tamba Kurkur Fm.	First mudstone interval	61.87	1.05	24.68	5.04	0.02	1.05	0.29	0.92	4.95	0.12	100.00	77.61	26.82	0.54
M14	18.7	Lower Triassic	Tamba Kurkur Fm.	First mudstone interval	62.70	0.97	24.03	4.95	0.02	1.13	0.26	0.79	5.04	0.11	100.00	77.51	30.24	0.55
69	19	Lower Triassic	Tamba Kurkur Fm.	First mudstone interval	61.30	1.04	24.94	5.27	0.02	1.17	0.26	0.92	4.95	0.12	100.00	77.94	27.12	0.55
70	20.4	Lower Triassic	Tamba Kurkur Fm.	First mudstone interval	58.00	1.00	23.98	9.52	0.11	1.35	0.41	0.92	4.60	0.11	100.00	77.44	26.04	0.74
0826M16	20.9	Lower Triassic	Tamba Kurkur Fm.	First mudstone interval	53.20	0.91	22.14	16.21	0.25	1.48	0.49	0.74	4.47	0.11	100.00	76.84	29.92	1.10
71	22.2	Lower Triassic	Tamba Kurkur Fm.	First mudstone interval	62.94	0.98	23.64	5.25	0.01	1.24	0.33	0.90	4.59	0.11	100.00	77.70	26.25	0.56
0826M17	22.25	Lower Triassic	Tamba Kurkur Fm.	First mudstone interval	61.62	0.98	23.85	5.22	0.03	1.44	0.89	0.85	5.01	0.11	100.00	74.49	28.14	0.60
M18	23.4	Lower Triassic	Tamba Kurkur Fm.	First mudstone interval	59.29	0.97	23.74	7.60	0.05	1.65	0.90	0.91	4.79	0.09	100.00	74.56	26.10	0.71
72	24	Lower Triassic	Tamba Kurkur Fm.	First mudstone interval	62.37	1.00	24.22	5.15	0.01	1.23	0.25	0.89	4.77	0.11	100.00	78.01	27.16	0.55
73	25.8	Lower Triassic	Tamba Kurkur Fm.	First mudstone interval	62.94	0.97	21.52	7.85	0.04	1.39	0.31	0.77	4.07	0.14	100.00	78.48	27.92	0.71
74	26.8	Lower Triassic	Tamba Kurkur Fm.	First mudstone interval	62.59	0.96	23.06	5.92	0.03	1.32	0.60	0.85	4.47	0.19	100.00	77.05	27.07	0.61
75	27.8	Lower Triassic	Tamba Kurkur Fm.	First mudstone interval	62.36	0.98	23.03	5.90	0.02	1.34	0.95	0.80	4.51	0.11	100.00	75.40	28.86	0.63
76	29	Lower Triassic	Tamba Kurkur Fm.	First mudstone interval	59.98	0.86	21.14	10.93	0.12	1.65	0.66	0.74	3.81	0.11	100.00	77.12	28.53	0.88
77	29.14	Lower Triassic	Tamba Kurkur Fm.	First mudstone interval	60.80	1.00	23.54	7.23	0.04	1.48	0.45	0.83	4.52	0.11	100.00	77.57	28.30	0.66
78	31.5	Lower Triassic	Tamba Kurkur Fm.	First mudstone interval	60.22	1.02	24.50	6.63	0.02	1.39	0.45	0.89	4.77	0.11	100.00	77.36	27.50	0.62
79	32.7	Lower Triassic	Tamba Kurkur Fm.	First mudstone interval	60.56	1.03	25.66	5.14	0.03	1.14	0.16	0.91	5.25	0.10	100.00	78.01	28.18	0.53
80	33.8	Lower Triassic	Tamba Kurkur Fm.	First mudstone interval	60.63	0.87	21.36	9.61	0.08	1.41	1.23	0.70	4.00	0.10	100.00	76.32	30.62	0.83
81	35.2	Lower Triassic	Tamba Kurkur Fm.	First mudstone interval	56.48	1.18	26.74	4.01	0.05	0.76	3.65	1.10	5.87	0.15	100.00	72.81	24.23	0.62
82	37.5	Lower Triassic	Tamba Kurkur Fm.	Second carbonate band	68.19	0.98	17.74	2.18	0.02	0.25	5.42	1.47	3.55	0.19	100.00	67.10	12.03	0.78
83	37.7	Lower Triassic	Tamba Kurkur Fm.	Second carbonate band	74.30	0.68	13.85	1.97	0.03	0.22	4.96	0.94	2.89	0.16	100.00	69.01	14.76	0.84
84	38.7	Lower Triassic	Tamba Kurkur Fm.	Second carbonate band	61.28	1.40	24.12	1.78	0.03	0.42	3.93	1.54	5.16	0.34	100.00	69.39	15.69	0.59
85	39.9	Lower Triassic	Tamba Kurkur Fm.	Second carbonate band	73.53	0.86	15.36	1.71	0.04	0.22	3.66	1.27	3.20	0.15	100.00	66.75	12.07	0.71
86	47	Lower Triassic	Tamba Kurkur Fm.	Third carbonate band	60.12	0.97	24.12	7.07	0.03	1.48	0.60	0.80	4.71	0.10	100.00	76.87	30.14	0.65
87	55.3	Upper Triassic	Mukut Fm.		58.29	1.16	28.18	3.85	0.01	1.04	0.74	1.66	5.00	0.07	100.00	75.15	16.98	0.48
88	57.4	Upper Triassic	Mukut Fm.		57.88	1.23	26.12	7.34	0.01	1.64	0.11	1.51	4.07	0.09	100.00	79.19	17.33	0.61
89	59.6	Upper Triassic	Mukut Fm.		57.55	1.22	24.20	9.75	0.01	2.30	0.17	1.24	3.47	0.10	100.00	80.50	19.56	0.75
90	60.9	Upper Triassic	Mukut Fm.		60.76	1.10	20.21	9.82	0.03	2.36	2.00	1.00	2.64	0.08	100.00	76.65	20.13	0.94